Supporting Information

Non-Conjugated Triarylamine-Based Intrinsic Microporous Polyamides for Electrochromic Supercapacitor: Diffusion Dynamics and Charge-Discharge Studies

By Yu-Jen Shao,[a†] Tzu-Chieh Yen,[a†] Chien-Chieh Hu,[b*] Guey-Sheng Liou [a*]

[a] Institute of Polymer Science and Engineering, National Taiwan University,
No. 1, Sec. 4, Roosevelt Rd., Taipei 10617, Taiwan. E-mail: gsliou@ntu.edu.tw

[b] Graduate Institute of Applied Science and Technology, National Taiwan University of Science and Technology, Taipei 106335, Taiwan. E-mail: cchu@mail.ntust.edu.tw

List of Contents for Supplementary Information:

Materials

The *N,N′*-bis(4-aminophenyl)-*N,N′*-di(4-methoxylphenyl)-*p*-phenylenediamine (**TPPA**, mp: 194-197 ℃) was synthesized according to the previous report. The supporting electrolyte of tetrabutylammonium tetrafluoroborate (TBABF4) was obtained by adding tetrabutylammonium (TBABr) aqueous solution dropwise into the saturated sodium tetrafluoroborate ($NaBF_4$) aqueous solution while stirring. The precipitated white solid was recrystallized with Ethanol/H2O (2:1, v/v) and dried under vacuum. And the commercially available calcium chloride (ACROS), pyridine (ACROS), 4,4′-oxydibenzoic acid (SIGMA), triphenyl phosphite (Acros), *N,N*-dimethylacetamide (TEDIA), 5-fluoro-2-nitrotoluene (Fluorochem), 1,4-diiodobenzene (Alfa Aesar), *o*-dichlorobenzene (Acros), copper (Acros), *p*-anisidine (Acros), 18-crown-6-ether (TCI), potassium carbonate (Alfa Aesar), Pd/C (Acros), hydrazine monohydrate (Alfa Aesar), dimethoxymethane (Acros) and other reagents were used as received.

Measurement

Glass capillary viscometers were used to measure the inherent viscosities of the polymers with the concentration of 0.5 g/dL DMAc in the Tamson TV2000 viscometer bath at 30 ℃. Molecular weights and polydispersity index (PDI) were obtained by gel permeation chromatographic (GPC) analysis on a Water chromatography unit interfaced with a 2410 refractive index detector. Two shodex GPC KD-803 and GPC KD-804 were connected in series with 20 mM LiCl in NMP solution as the eluent at the flow rate of 0.35 mL/min at 40 °C calibrated with polystyrene standards. Thermal properties were conducted by thermogravimetric analysis (TGA) with TA Instruments Q50 and differential scanning calorimeter (DSC) with TA instruments Q-20. 3 to 8 mg of the prepared polymer samples were used for the TGA measurements in flowing

nitrogen and air (flow rate: 60 mL/min) atmosphere at a heating rate of 20 °C/min. Transparency and color coordination of the polymer films was measured by JASCO V650 and HITACHI U4100 UV-vis spectrophotometer, and Agilent recorded the absorbance spectrum of switching time. Electrochemical properties, including cyclic voltammetry (CV), differential pulse voltammetry (DPV), and electrochemical impedance spectroscopy (EIS), were conducted through CH Instrument 6122E Electrochemical Analyzer under a three-electrode system polymer-casted ITO glass as a working electrode, an Ag/AgCl reference electrode, and a platinum counter electrode in 3 mL of anhydrous acetonitrile with 0.1 M $TBABF_4$ as supporting electrolyte under the air atmosphere. The scanning rate of CV was set from 10 mV/s to 200 mV/s to investigate the diffusivities of each polymer. Wide-angle X-ray diffractometry (WXRD) was conducted on BRUKER, D8 DISCOVER SSS Multi-Function High Power X-Ray diffractometer with CuKα (wavelength: 1.54 Å) radiation.

Preparation of the polymeric electrode

The electrodes were prepared for all the electrochemical measurements by drop-casting on the 3 cm × 2.5 cm ITO glass with 400 μL solution with 2 mg of the resulting polymer in 1 mL DMAc. After dropping on the ITO glass, most of the solvent was removed in the vacuum oven at 50 ℃. Then, the temperature was raised to 120 ℃/2 h and 180 ℃/2 h in a vacuum to ensure all the solvent was removed. The 3 cm × 2.5 cm ITO glass with polymer film was further cut to the desired size for each measurement.

Theoretical Calculation

The molecular simulations in this study were carried out by Gaussian 09 program package. The molecular geometric optimization of the model compounds and the model

units of polyimides was calculated by the density functional theory (DFT) B3LYP with the 6-31G(d,p) basic set.

Experimental methods

Synthesis of Diamine Monomer (TPPA-Me)

***N*-(4-methoxyphenyl)-3-methyl-4-nitroaniline (DPA-Me)**

The mixture of 25.4 g (0.206 mol) of *p*-anisidine, 24 mL (0.197 mol) of 4-fluoro-2-methyl-1-nitrobenzene, and 12 mL of triethylamine was added to 140 mL of dimethyl sulfoxide (DMSO) in sequence, then was stirred at 90 ℃ for 12 h. The solution was precipitated by water, and then the collected crude product was recrystallized by MeOH/H_2O (500 mL/200 mL) to gain a yellow-brown needle-like crystal. After being collected by filtration and dried in a vacuum at 80 ℃ to afford 33.58 g (66% in yield) of yellow-brown crystal with m.p of 119-121 ℃. ^{1}H-NMR (500 MHz, DMSO-d_6) δ: 2.50 (s, 3H), 3.75(s, 3H), 6.71 (s, 1H), 6.75 (d, 1H), 6.96 (d, 2H), 7.15 (d, 2H), 7.98 (s, 1H), 8.90 (d, 1H); ^{13}C-NMR (125 MHz, DMSO-d_6) δ: 21.9, 55.2, 110.8, 114.7, 115.2, 123.8, 128.0, 132.7, 137.0, 150.8, 155.9; Anal. Calcd (%) for $C_{14}H_{14}N_2O_3$: C, 65.11; H, 5.46; N, 10.85. Found: C, 64.86; H, 5.43; N, 10.76.

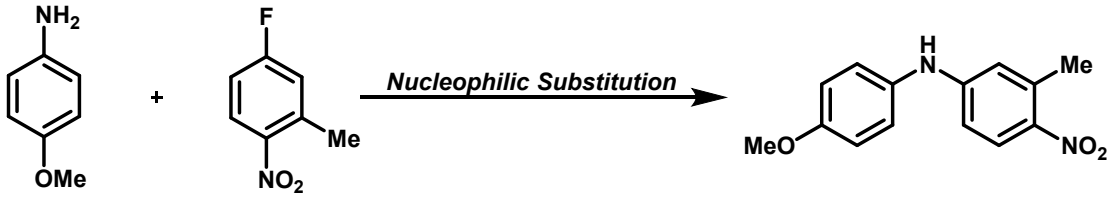

Scheme S1. The synthetic route for *N*-(4-methoxyphenyl)-3-methyl-4-nitroaniline (**DPA-Me**).

***N*,*N*′-Bis(3-methyl-4-nitrophenyl)-*N*,*N*′-*di*(4-methoxyphenyl)-*p*-phenylenediamine (TPPA-Me dinitro)**

The copper powder (1.2 g, 18.9 mmol), 1,4-diiodobenzene (2.64 g, 8 mmol), **DPA-Me** (4.65 g, 18 mmol), and anhydrous potassium carbonate (4.5 g, 32.6 mmol) were added into the flask with the 18-crown-6-ether (1 g, 3.78 mmol) dissolved 1,2-dichlorobenzene (15 mL). The reaction mixture was refluxed for 48 h, then filtrated and purified by column chromatography with an eluent of dichloromethane/hexane (1:1) to afford a light red crystal compound with a yield of 45% with m.p of 233-235 ℃; ^{1}H-NMR (500 MHz, DMSO-d_6) δ: 2.44 (s, 6H), 3.78(s, 6H), 6.65 (s, 2H), 6.68 (d, 2H), 7.03(d, 4H), 7.22 (d, 4H), 7.23 (d, 4H), 7.97 (d, 2H); ^{13}C-NMR (125 MHz, DMSO-d_6) δ: 21.5, 55.4, 115.0, 115.6, 119.4, 127.3, 127.4, 128.9, 136.2, 137.5, 139.6, 142.2, 152.2, 157.7; Anal. Calcd (%) for $C_{34}H_{30}N_4O_6$: C, 69.14; H, 5.12; N, 9.49. Found: C, 68.82; H, 4.97; N, 9.40.

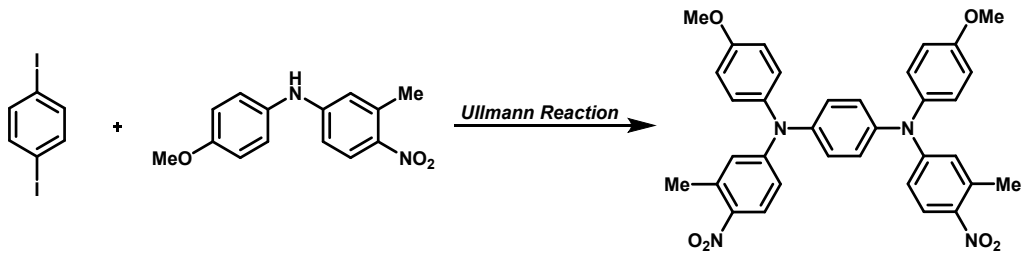

Scheme S2. The synthetic route of *N*,*N*′-bis(3-methyl-4-nitrophenyl)-*N*,*N*′-*di*(4-methoxyphenyl)-*p*-phenylene diamine (**TPPA-Me dinitro**).

N,*N*′-Bis(3-methyl-4-aminophenyl)-*N*,*N*′-*di*(4-methoxyphenyl)-*p*-phenylenediamine (TPPA-Me)

The new TPPA-based diamine monomer *N*,*N*′-bis(3-methyl-4-aminophenyl)-*N*,*N*′-*di*(4-methoxyphenyl)-*p*-phenylenediamine (**TPPA-Me**) was synthesized by Pd/C-catalyzed hydrazine reduction of nitro-compound *N*,*N*′-Bis(3-methyl-4-aminophenyl)-*N*,*N*′-*di*(4-methoxyphenyl)-*p*-phenylenediamine. To a mixture of **TPPA-Me dinitro** compound (1.18 g, 2 mmol), Pd/C (0.12 g, 10 wt%) in 20 mL EtOH/THF (1:1, v/v), hydrazine monohydrate was added dropwise, and the reaction refluxed for 4 h. The

solution was filtrated by celite to remove Pd/C, and then concentrated under reduced pressure. The product was recrystallized by EtOH, resulting in a 90% yield with m.p of 209-210 ℃; ^{1}H-NMR (500 MHz, DMSO-d_6) δ: 2.07 (s, 6H), 3.69(s, 6H), 4.45 (s, 4H), 6.52 (s, 2H), 6.57(d, 4H), 6.66 (d, 2H), 6.78 (d, 2H), 6.93 (d, 4H); ^{13}C-NMR (125 MHz, DMSO) δ: 17.4, 55.1, 114.5, 114.8, 121.6, 123.7, 124.4, 127.7, 136.5, 141.7, 142.0, 143.2, 154.0; Anal. Calcd (%) for $C_{34}H_{34}N_4O_2$: C, 76.95; H, 6.46; N, 10.56. Found: C, 76.26; H, 6.41; N, 10.48.

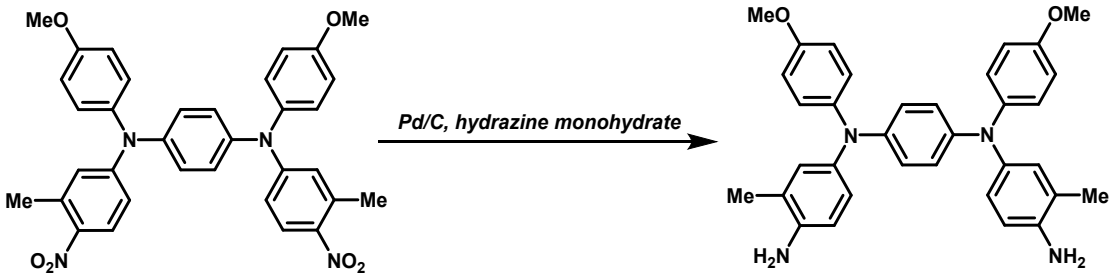

Scheme S3. The synthetic route of *N*,*N*′-Bis(3-methyl-4-aminophenyl)-*N*,*N*′-*di*(4-methoxyphenyl)-*p*-phenylene diamine (**TPPA-Me**).

Synthesis of Polyamides

This study synthesized a series of novel aromatic TPPA-based polyamides via direct polycondensation of diamines of **TPPA** and **TPPA-Me** with 4,4'-oxybis(benzoic acid) and Tröger's base dicarboxylic acid, individually, as shown in **Scheme S4**. Their synthetic routes are described as follows, and the resulting molecular weights and solubility properties are summarized in **Table S1** and **Table S2**.

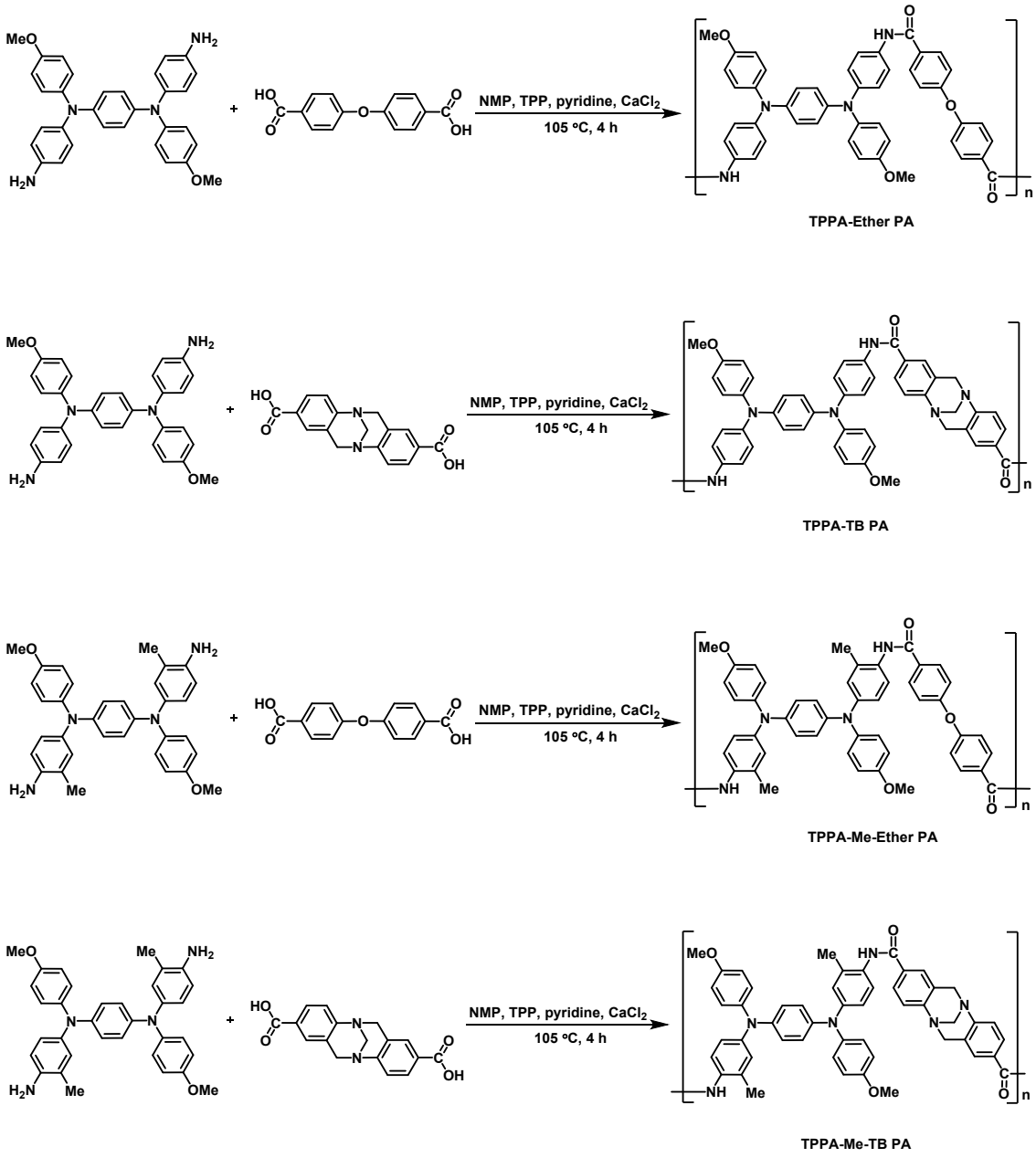

Scheme S4. Synthetic routes of prepared arylamine-based polyamides.

Preparation of Arylamine-based Polyamides

The dicarboxylic acid (0.5 mmol) was added to 1 mL NMP (20 wt%), then 0.5 mL pyridine, 0.03 g $CaCl_2$, 0.4 mL TPP and TPPA diamine (0.5 mmol) were added to the solution. The mixture was reacted at 105 °C for 4 hours. After cooling to room temperature, the solution was poured into the methanol/water (1:1, v/v) mixture to

obtain fiber-like precipitation of the polymer. The precipitated polymer was filtered and purified by Soxhlet extraction by methanol and water for 24 hours, respectively.

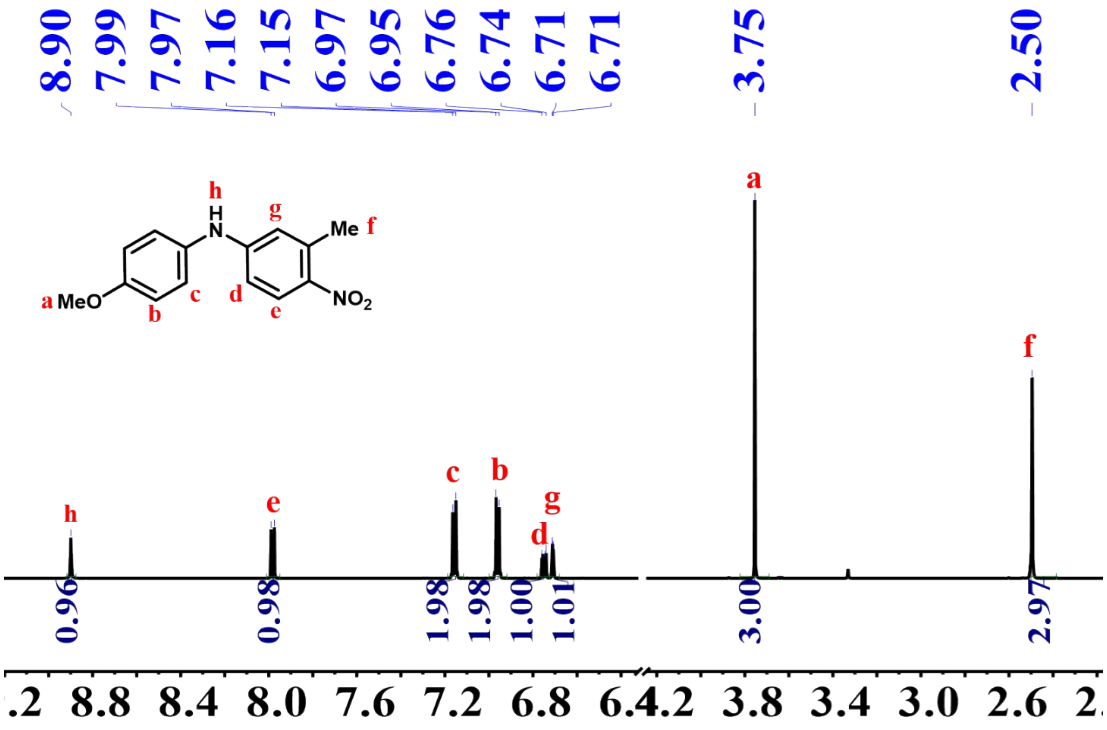

Fig. S1. ^{1}H NMR spectrum of **DPA-Me** in DMSO-d_6.

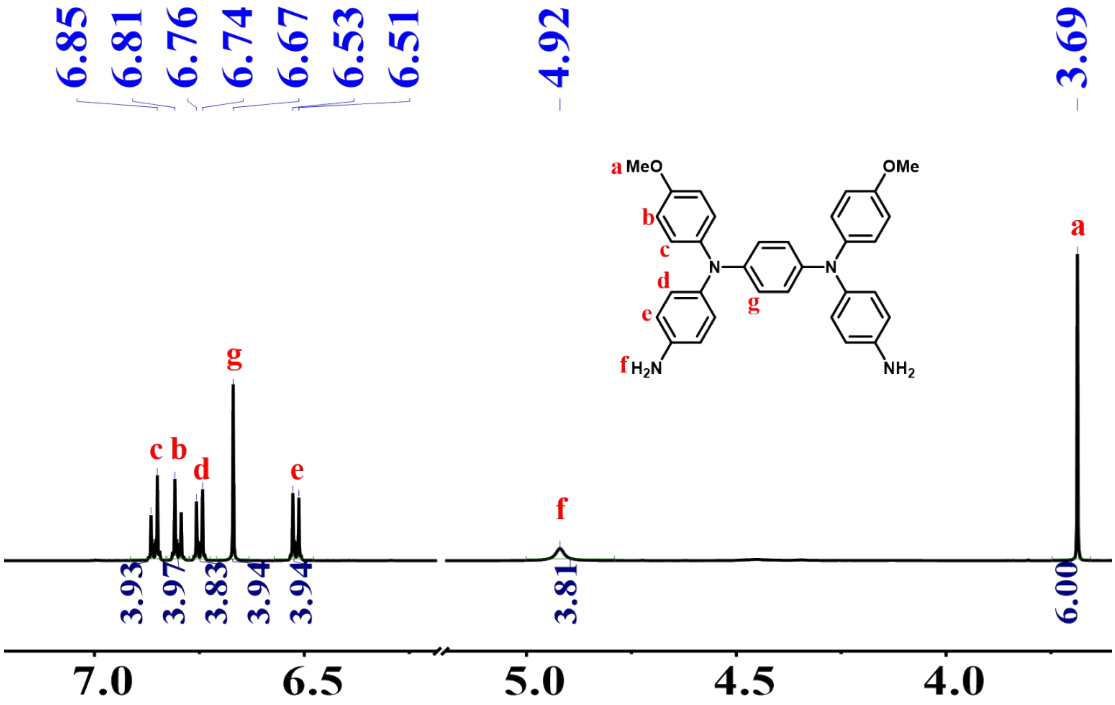

Fig. S2. ^{1}H NMR spectrum of **TPPA** in DMSO-d_6.

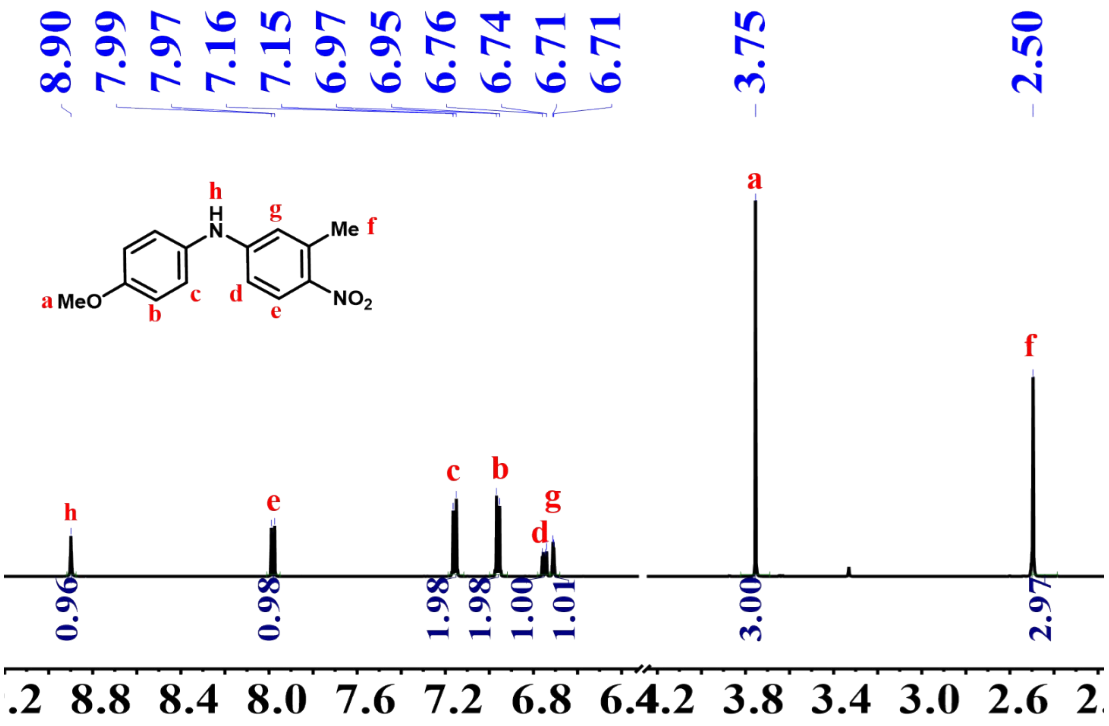

Fig. S3. [1]H NMR spectrum of **DPA-Me** in DMSO-d_6.

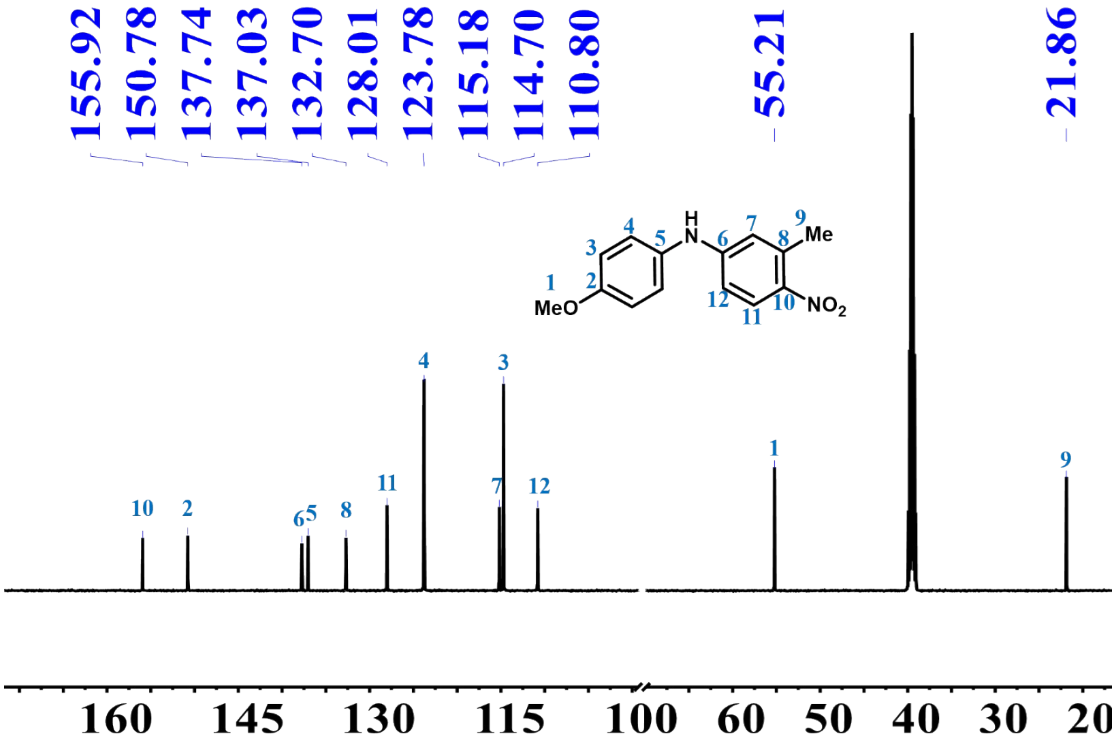

Fig. S4. [13]C NMR spectrum of **DPA-Me** in DMSO-d_6.

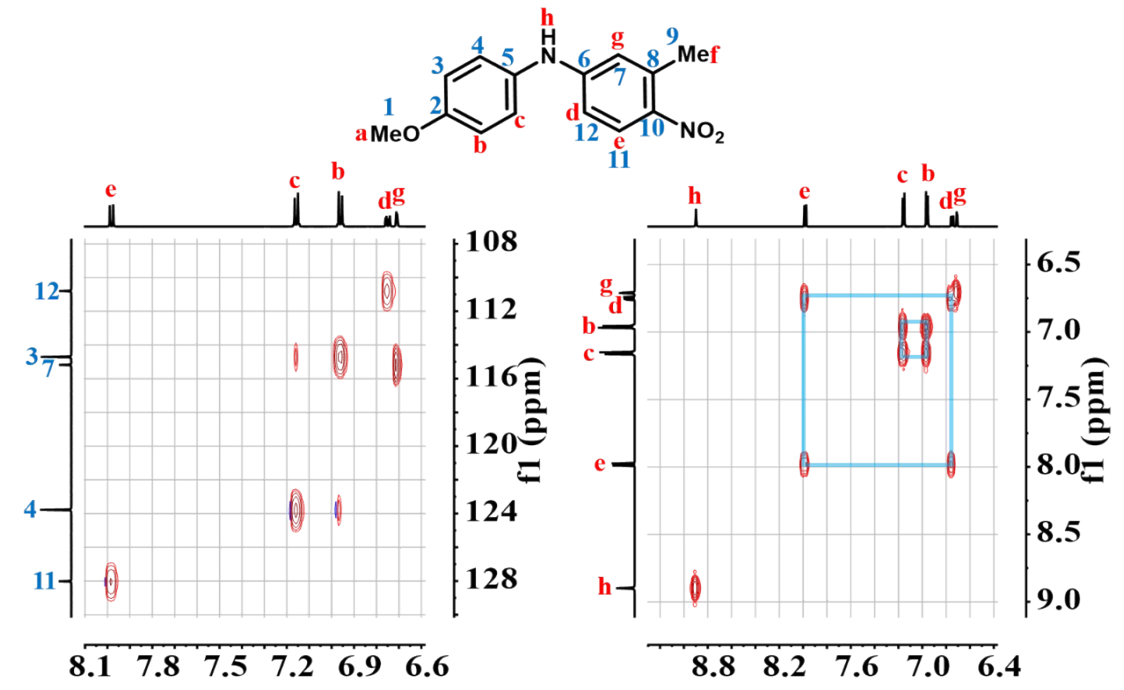

Fig. S5. ^{13}C-^{1}H HSQC and ^{1}H-^{1}H COSY NMR spectra of **DPA-Me** in DMSO-d_6.

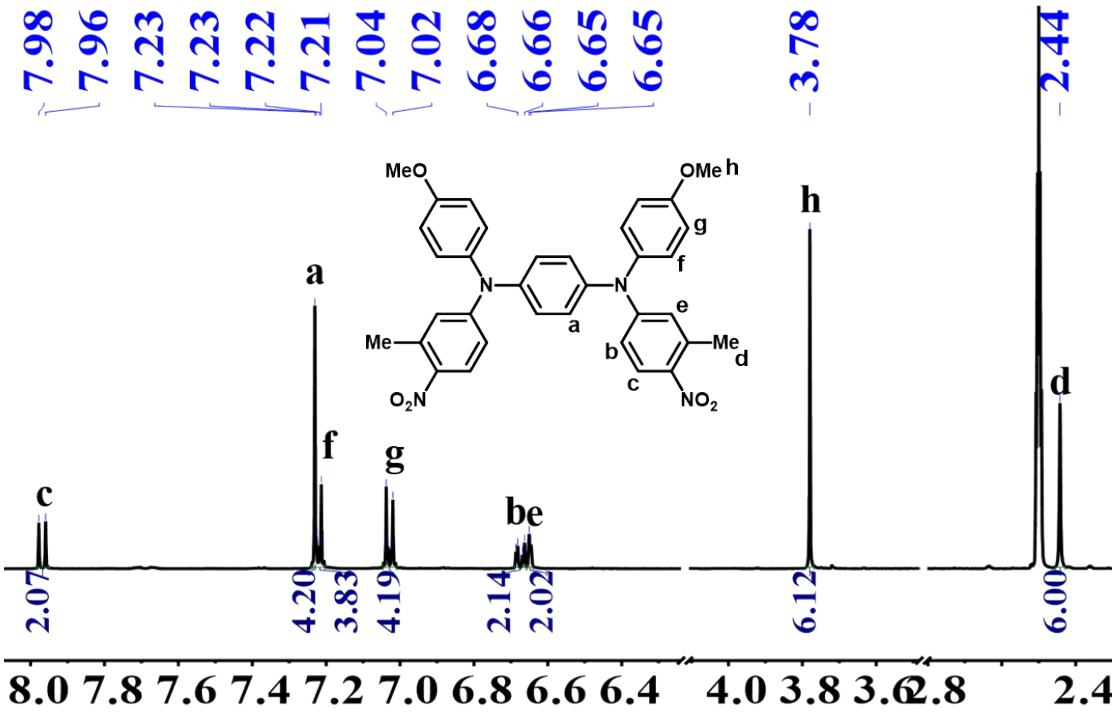

Fig. S6. ^{1}H NMR spectrum of **TPPA-Me** dinitro in DMSO-d_6.

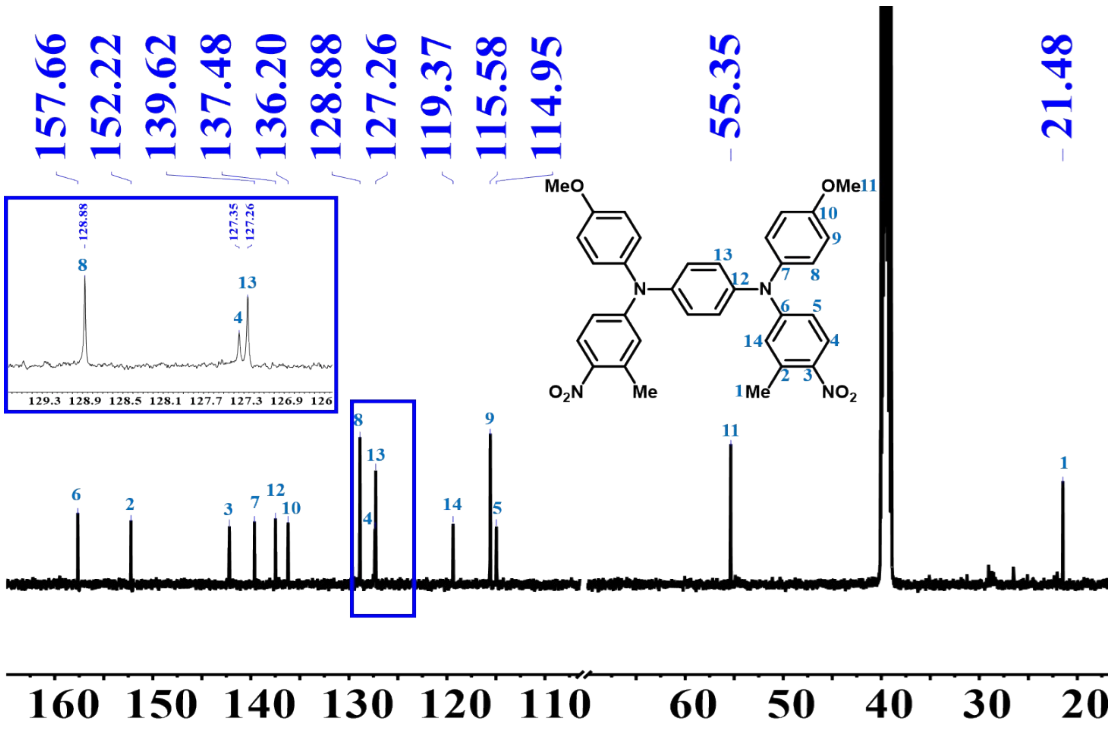

Fig. S7. ^{13}C NMR spectrum of **TPPA-Me** dinitro in DMSO-d_6.

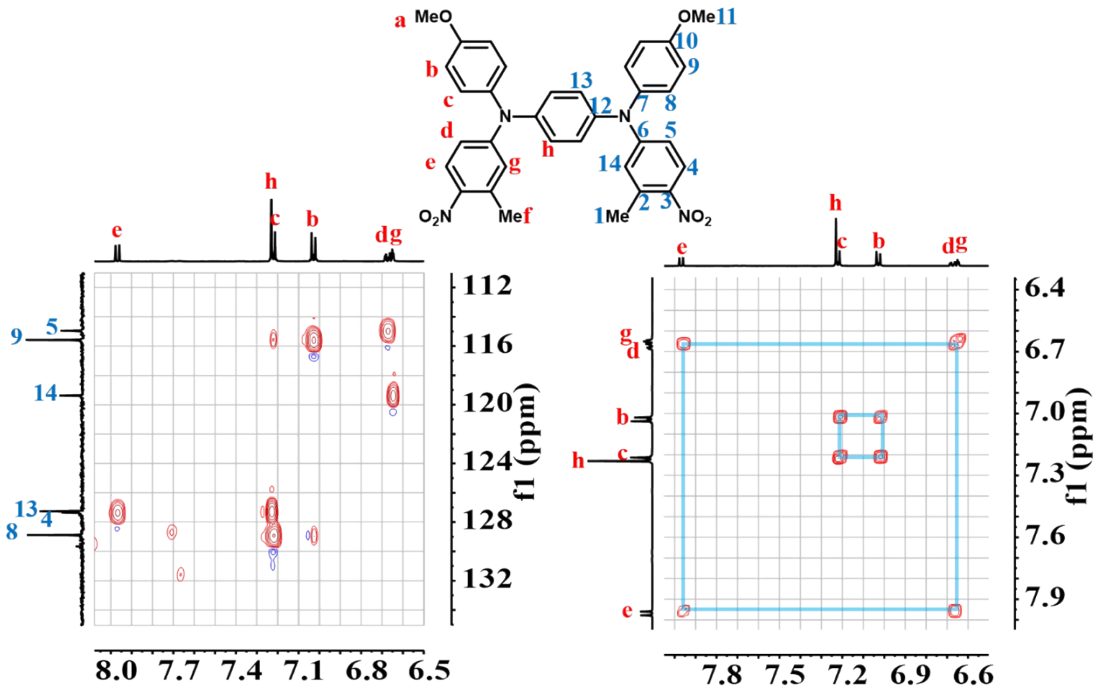

Fig. S8. ^{13}C-^{1}H HSQC and ^{1}H-^{1}H COSY NMR spectra of **TPPA-Me** dinitro in DMSO-d_6.

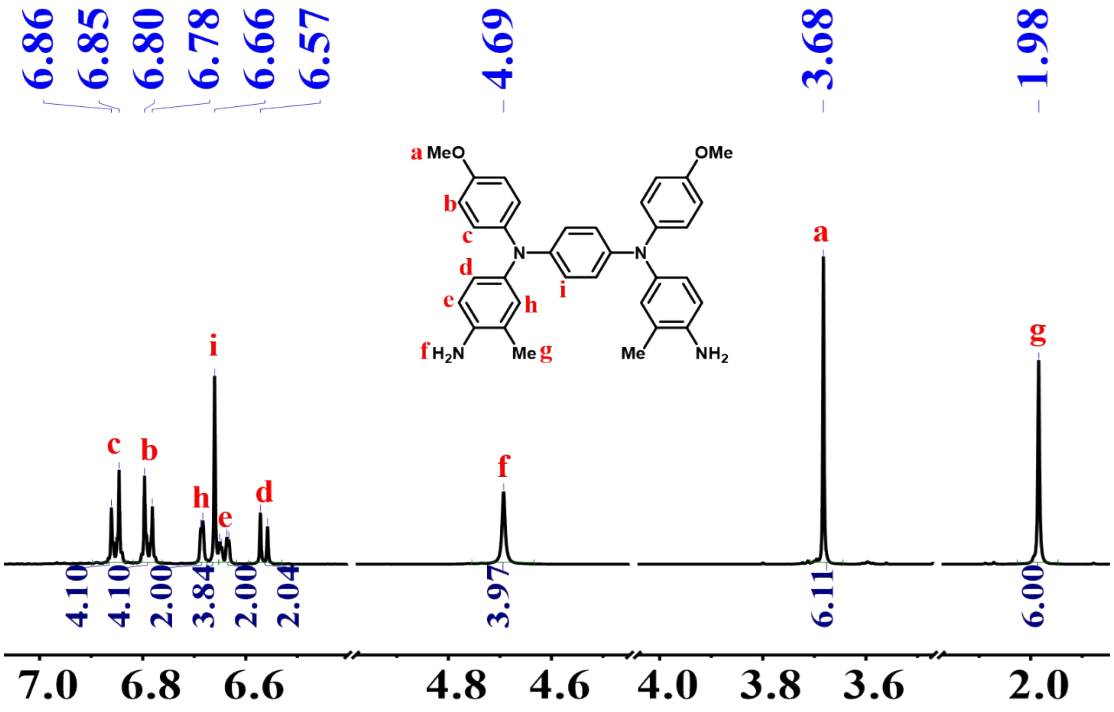

Fig. S9. ^{1}H NMR spectrum of **TPPA-Me** in DMSO-d_6.

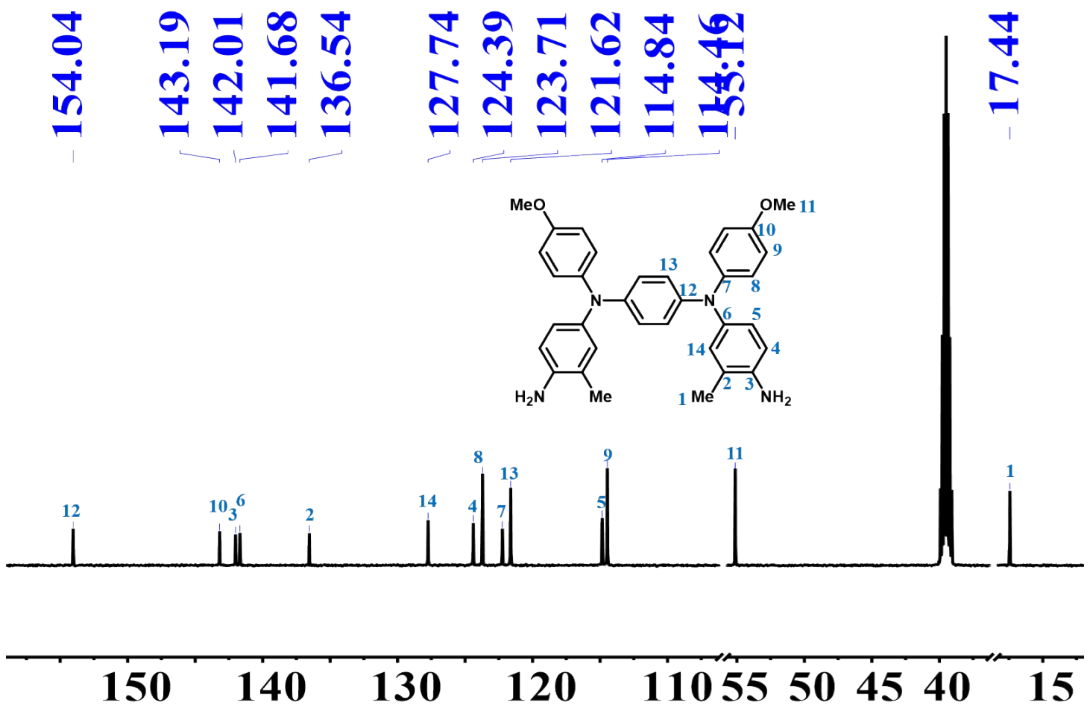

Fig. S10. ^{13}C NMR spectrum of **TPPA-Me** in DMSO-d_6.

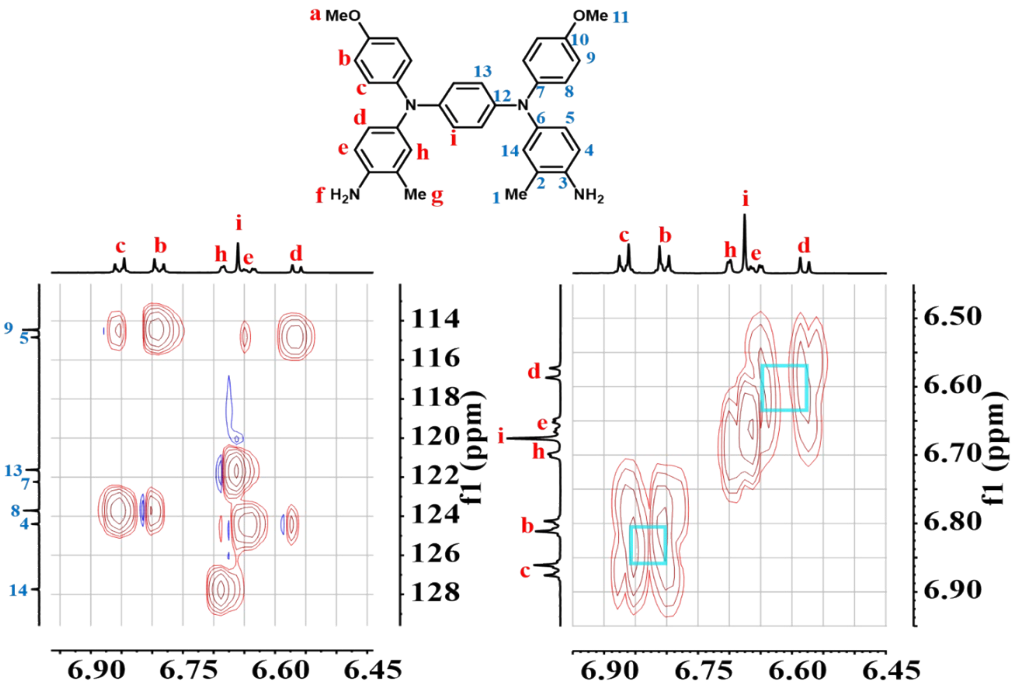

Fig. S11. ^{13}C-^{1}H HSQC and ^{1}H-^{1}H COSY NMR spectra of **TPPA-Me** in DMSO-d_6.

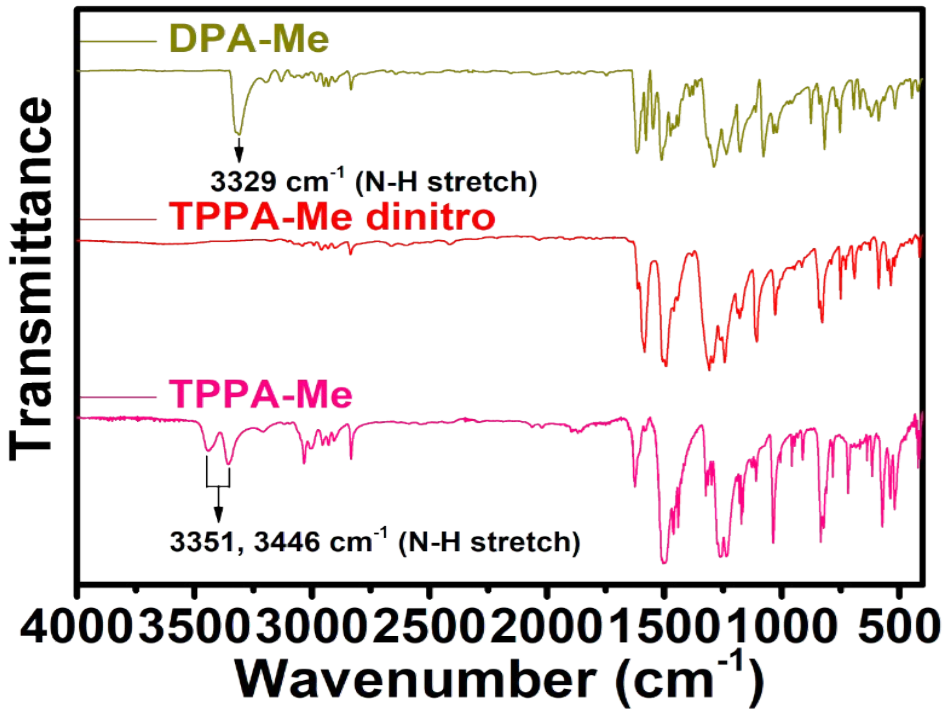

Fig. S12. FT-IR spectra of **DPA-Me**, **TPPA-Me dinitro**, and **TPPA-Me**.

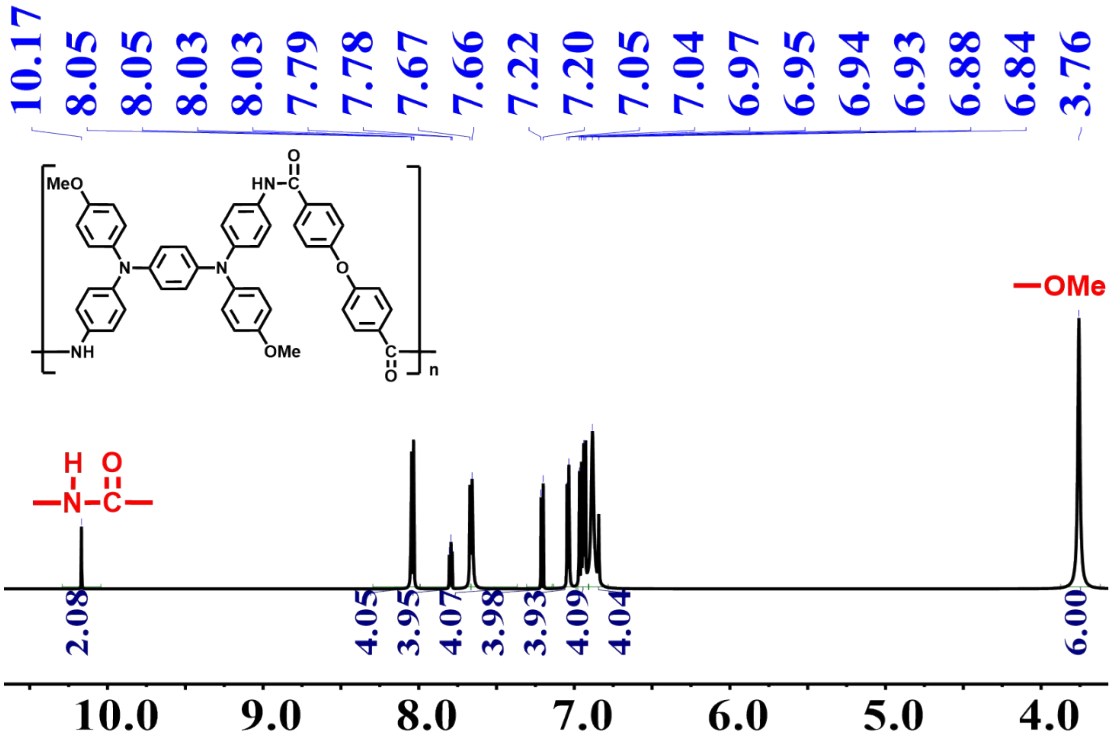

Fig. S13. ^{1}H NMR spectrum of **TPPA-Ether** in DMSO-d_6.

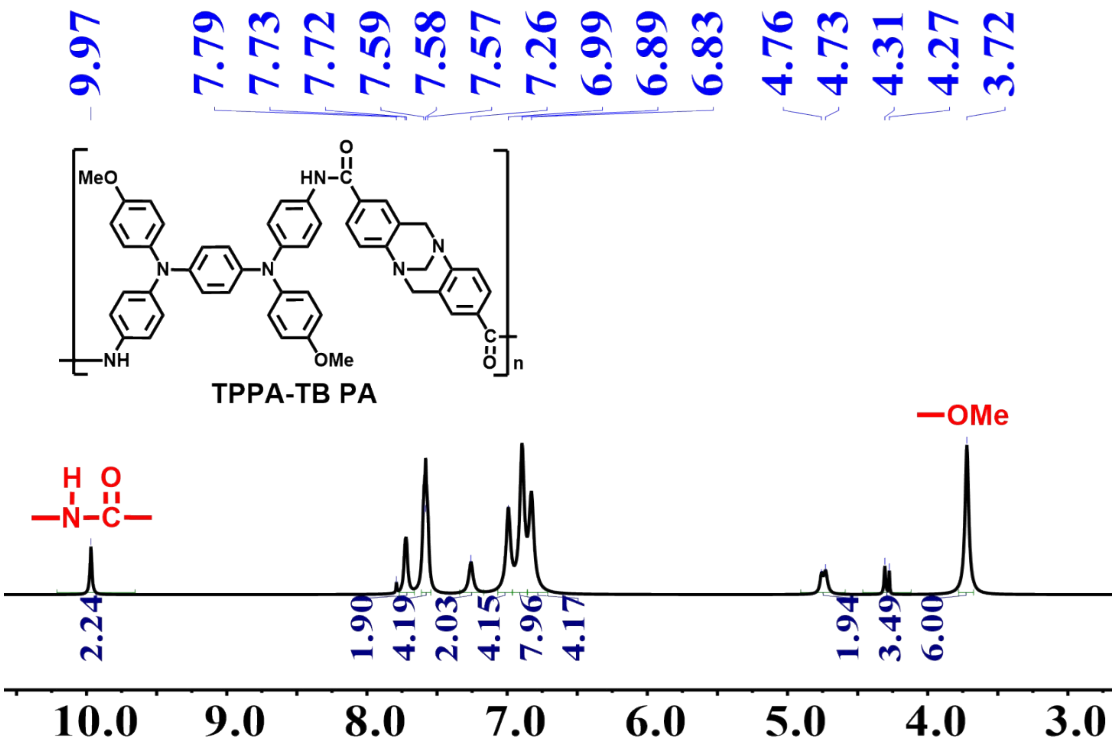

Fig. S14. ^{1}H NMR spectrum of **TPPA-TB** in DMSO-d_6.

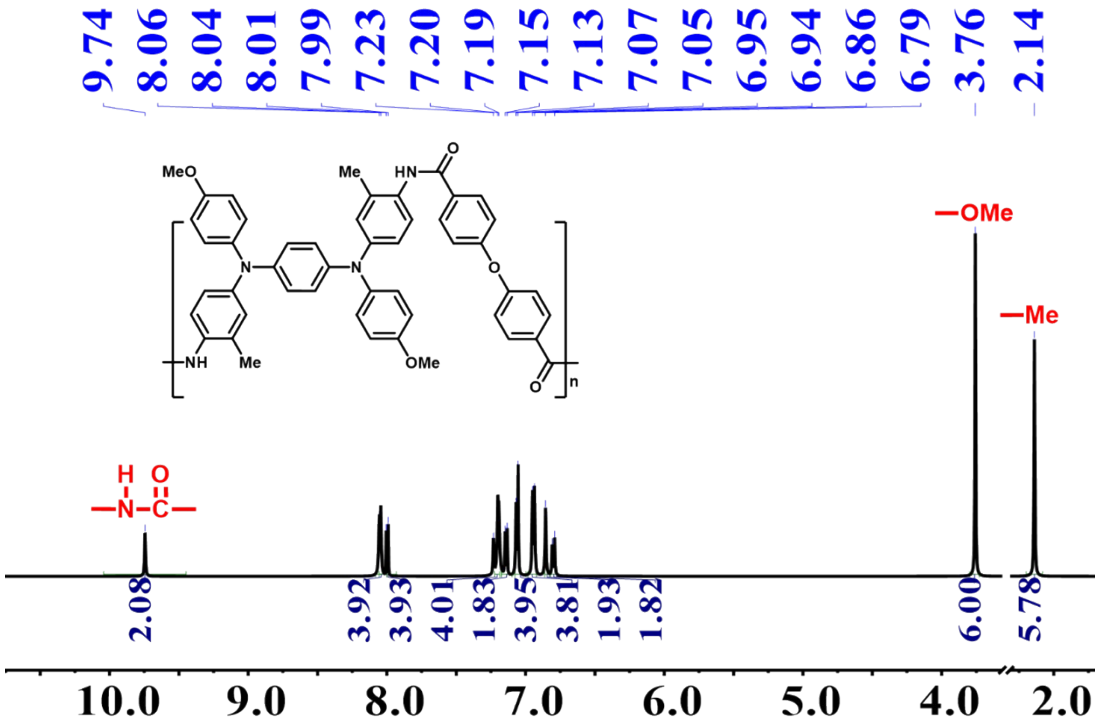

Fig. S15. [1]H NMR spectrum of **TPPA-Me-Ether** in DMSO-d_6.

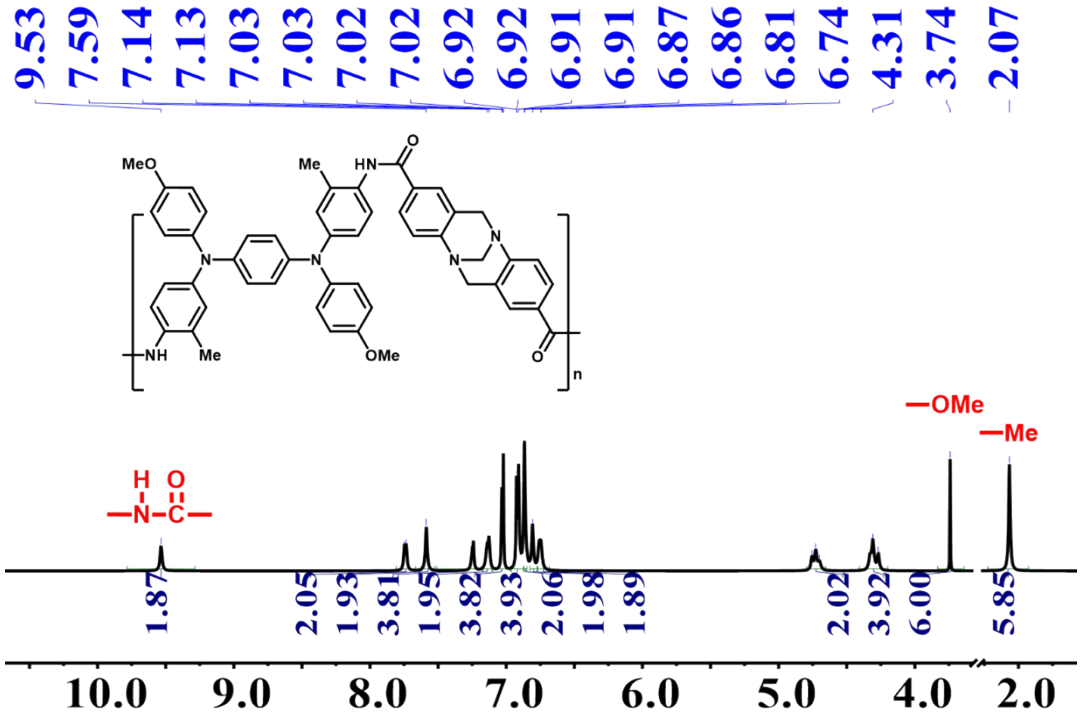

Fig. S16. [1]H NMR spectrum of **TPPA-Me-TB** in DMSO-d_6.

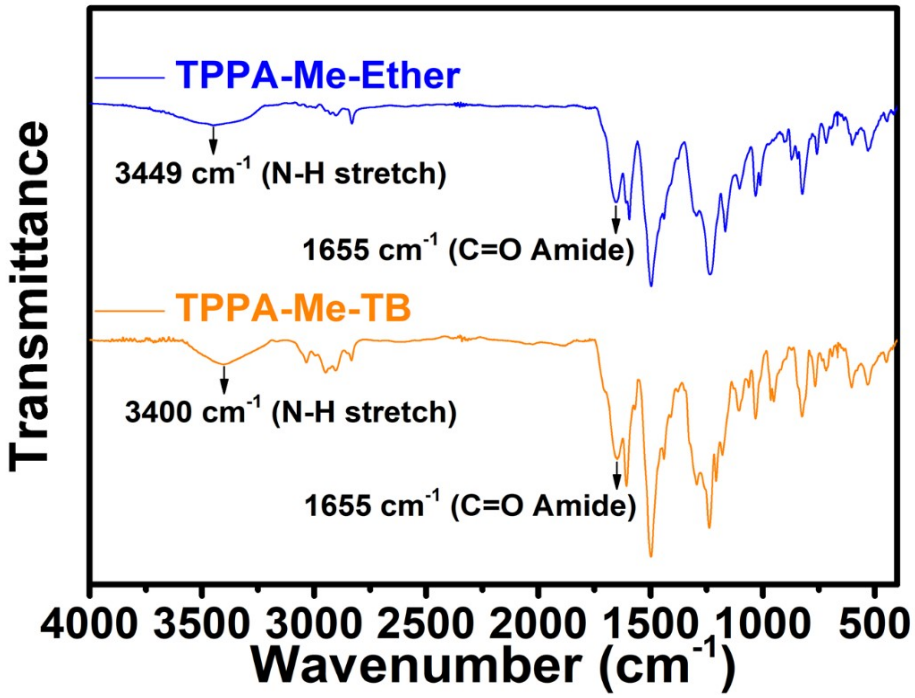

Fig. S17. FT-IR spectra of **TPPA-Me-Ether** and **TPPA-Me-TB**.

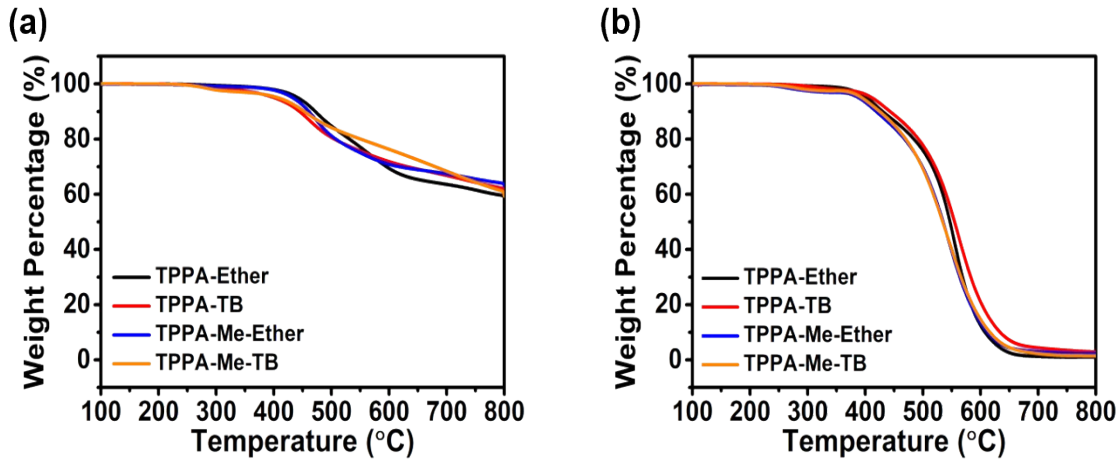

Fig. S18. TGA curves of prepared polymers under (a) nitrogen and (b) air atmosphere.

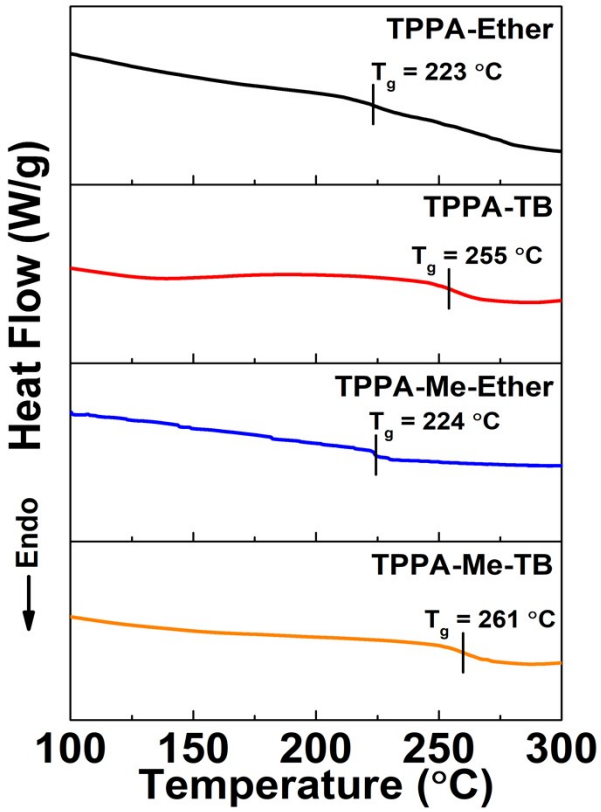

Fig. S19. DSC trace of TPPA-based polymers at the heating rate of 20 °C/min in a nitrogen atmosphere.

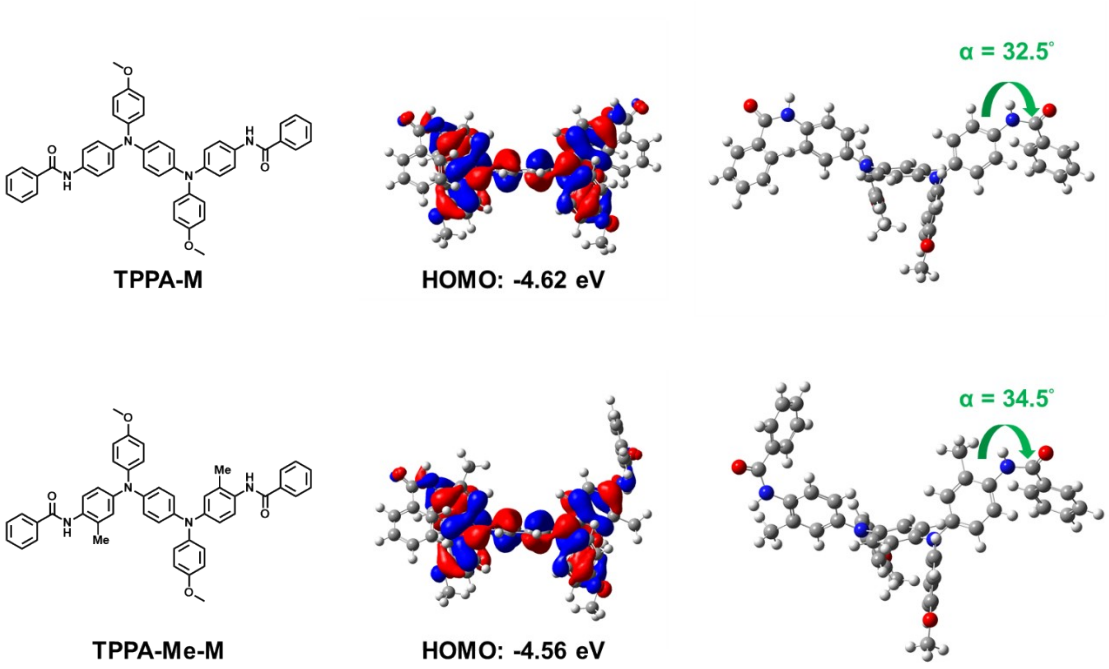

Fig. S20. Theoretical calculation of **TPPA-M** and **TPPA-Me-M** by using the DFT method at B3LYP/6-31G(d,p) level.

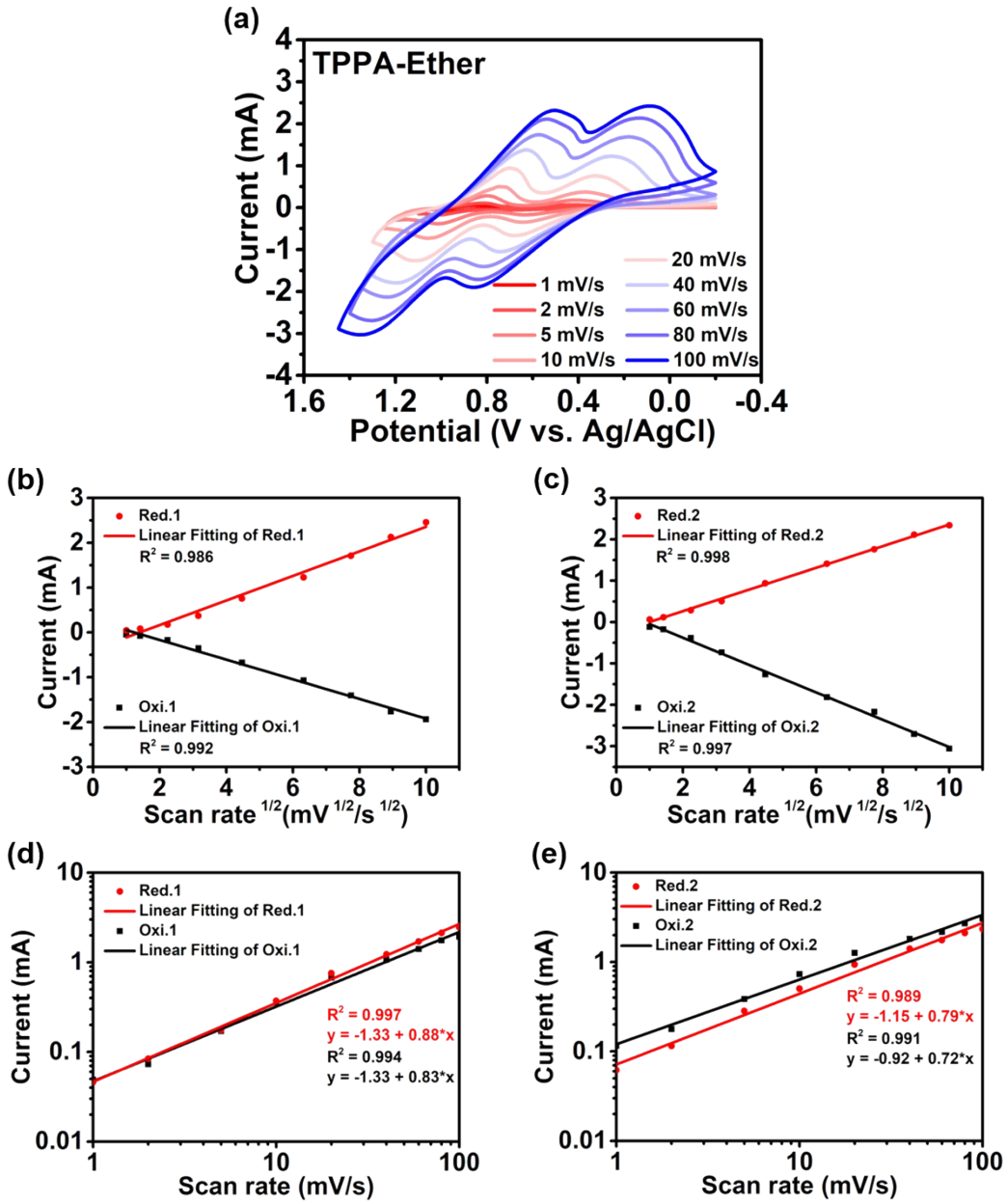

Fig. S21. (a) Cyclic voltammetric diagram and plots of **TPPA-Ether** of (b) peak current density of first oxidation state versus square root of scan rate, (c) peak current density of second oxidation state versus square root of scan rate, (d) peak current density of first oxidation state versus scan rate in logarithm scale, (e) peak current density of second oxidation state versus scan rate in logarithm scale at different scan rates between 10 to 200 mV/s.

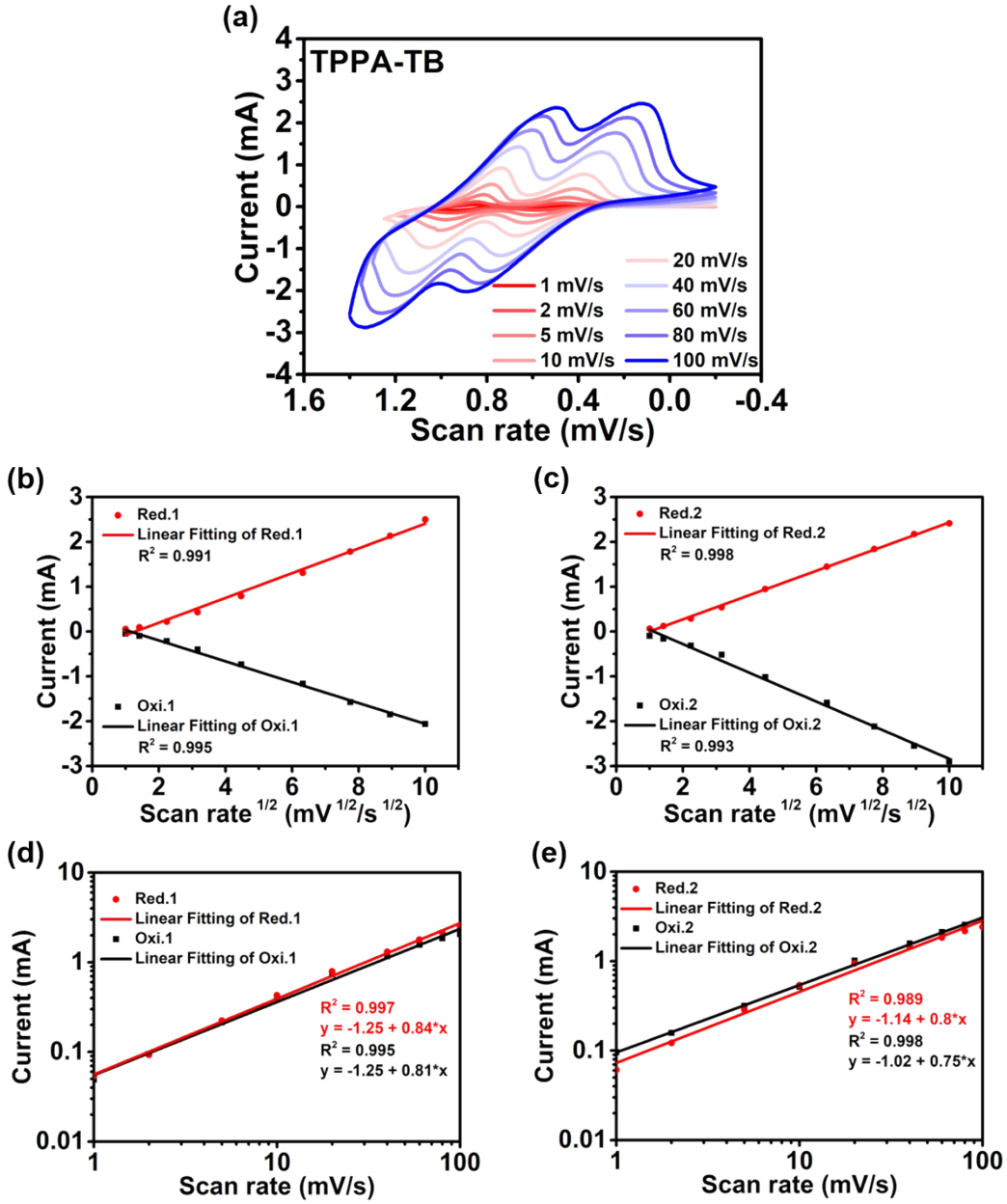

Fig. S22. (a) Cyclic voltammetric diagram and plots of **TPPA-TB** of (b) peak current density of first oxidation state versus square root of scan rate, (c) peak current density of second oxidation state versus square root of scan rate, (d) peak current density of first oxidation state versus scan rate in logarithm scale, (e) peak current density of second oxidation state versus scan rate in logarithm scale at different scan rates between 10 to 200 mV/s.

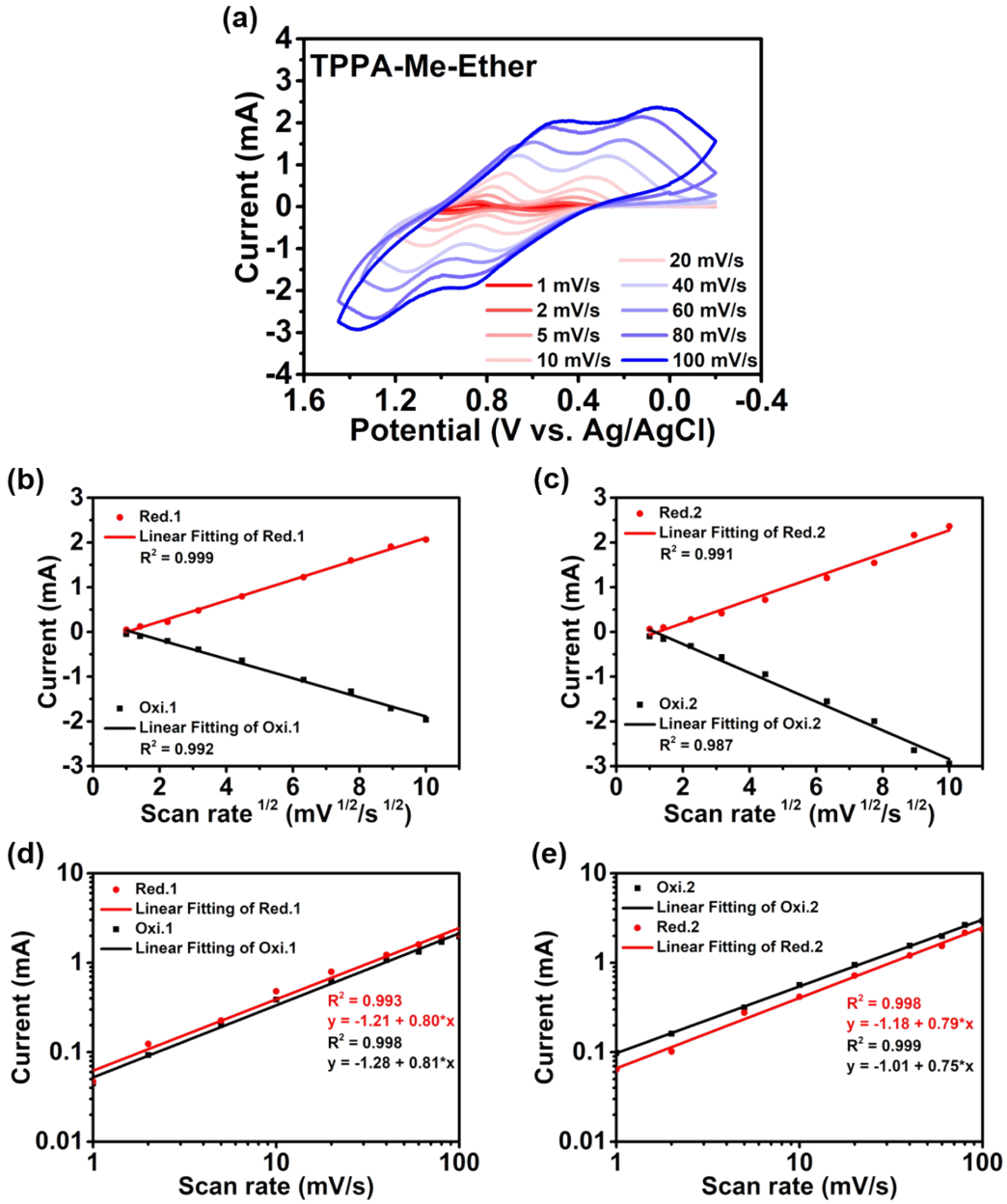

Fig. S23. (a) Cyclic voltammetric diagram and plots of **TPPA-Me-Ether** of (b) peak current density of first oxidation state versus square root of scan rate, (c) peak current density of second oxidation state versus square root of scan rate, (d) peak current density of first oxidation state versus scan rate in logarithm scale, (e) peak current density of second oxidation state versus scan rate in logarithm scale at different scan rates between 10 to 200 mV/s.

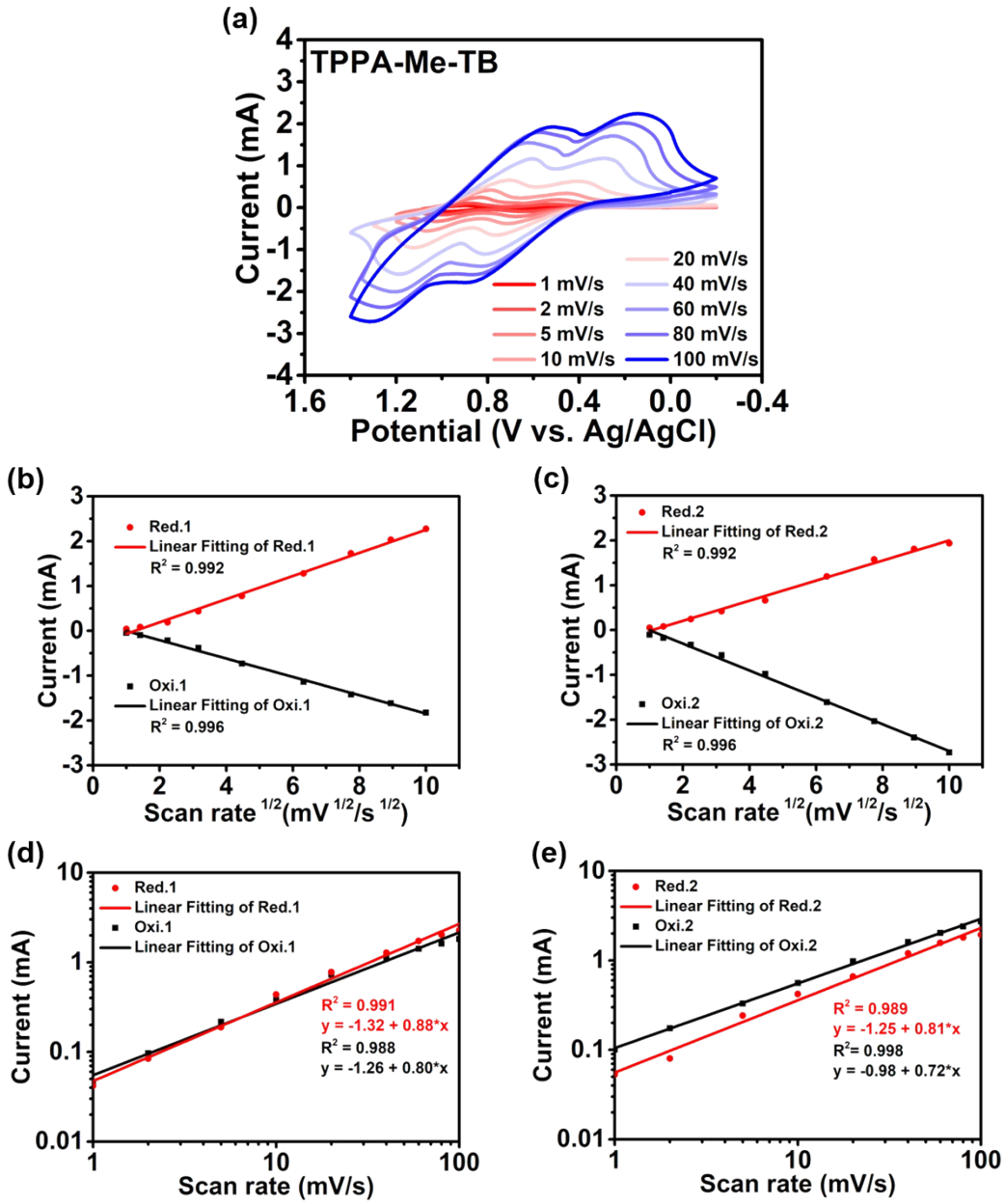

Fig. S24. (a) Cyclic voltammetric diagram and plots of **TPPA-Me-TB** of (b) peak current density of first oxidation state versus square root of scan rate, (c) peak current density of second oxidation state versus square root of scan rate, (d) peak current density of first oxidation state versus scan rate in logarithm scale, (e) peak current density of second oxidation state versus scan rate in logarithm scale at different scan rates between 10 to 200 mV/s.

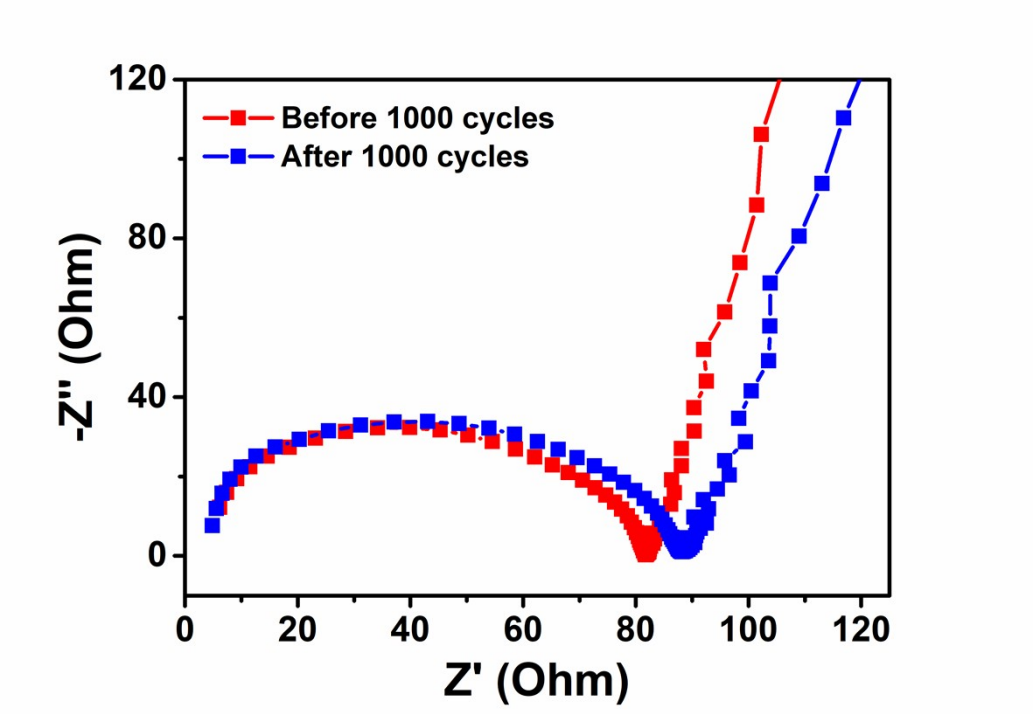

Fig. S25. Nyquist plot of **TPPA-Me-TB** before and after 1000 cycles of CV scanning.

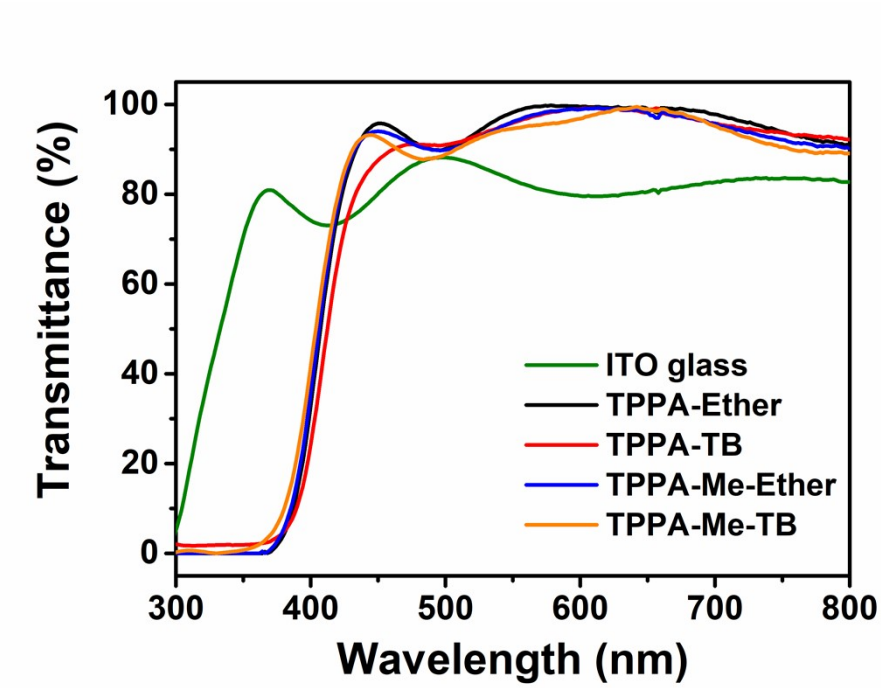

Fig. S26. UV-vis spectra of ITO glass (air as background) and the resulting polyamides (ITO glass as background, thickness: 350 ± 30 nm).

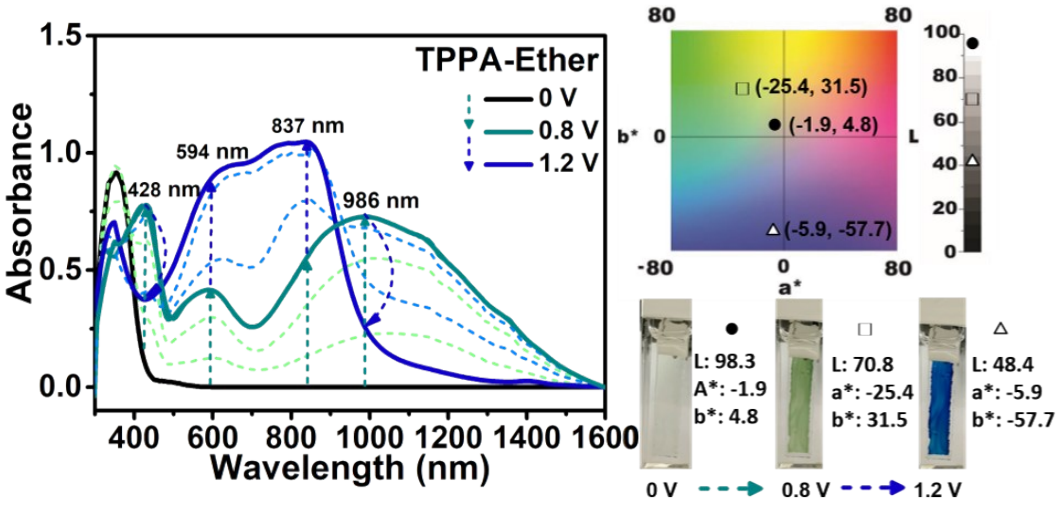

Fig. S27. Spectroelectrochemical spectra and the analysis of CIELAB color space for **TPPA-Ether** measured on the ITO-coated glass substrate in 0.1 M $TBABF_4$/MeCN.

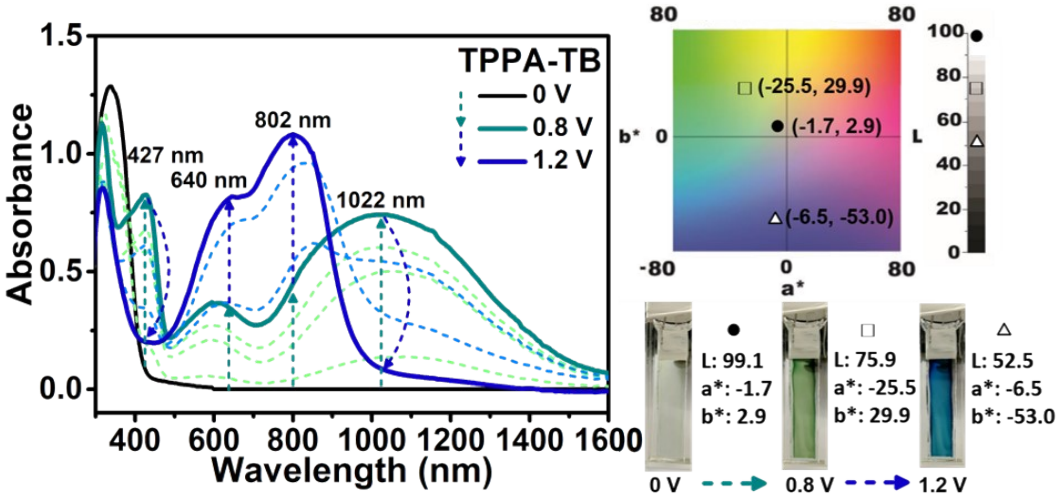

Fig. S28. Spectroelectrochemical spectra and the analysis of CIELAB color space for **TPPA-TB** measured on the ITO-coated glass substrate in 0.1 M $TBABF_4$/MeCN.

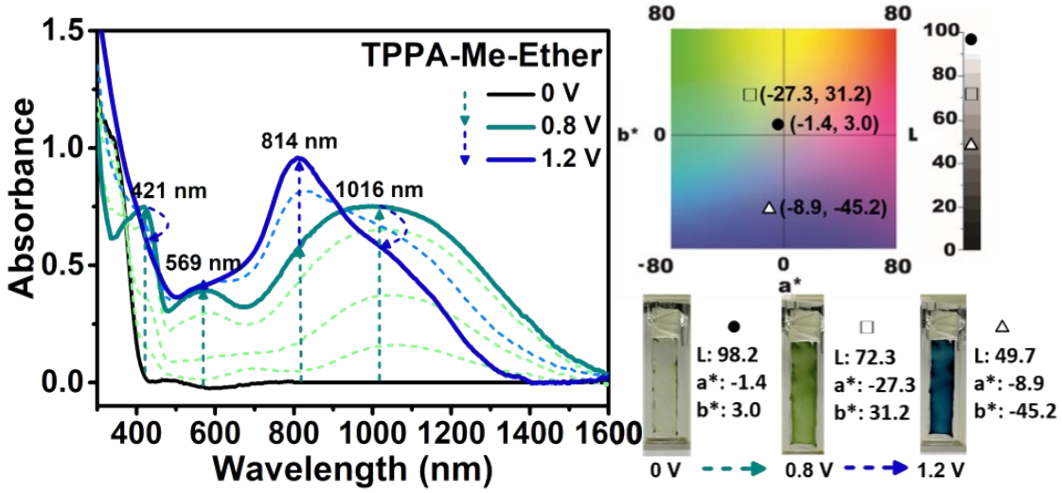

Fig. S29. Spectroelectrochemical spectra and the analysis of CIELAB color space for **TPPA-Me-Ether** measured on the ITO-coated glass substrate in 0.1 M $TBABF_4$/MeCN.

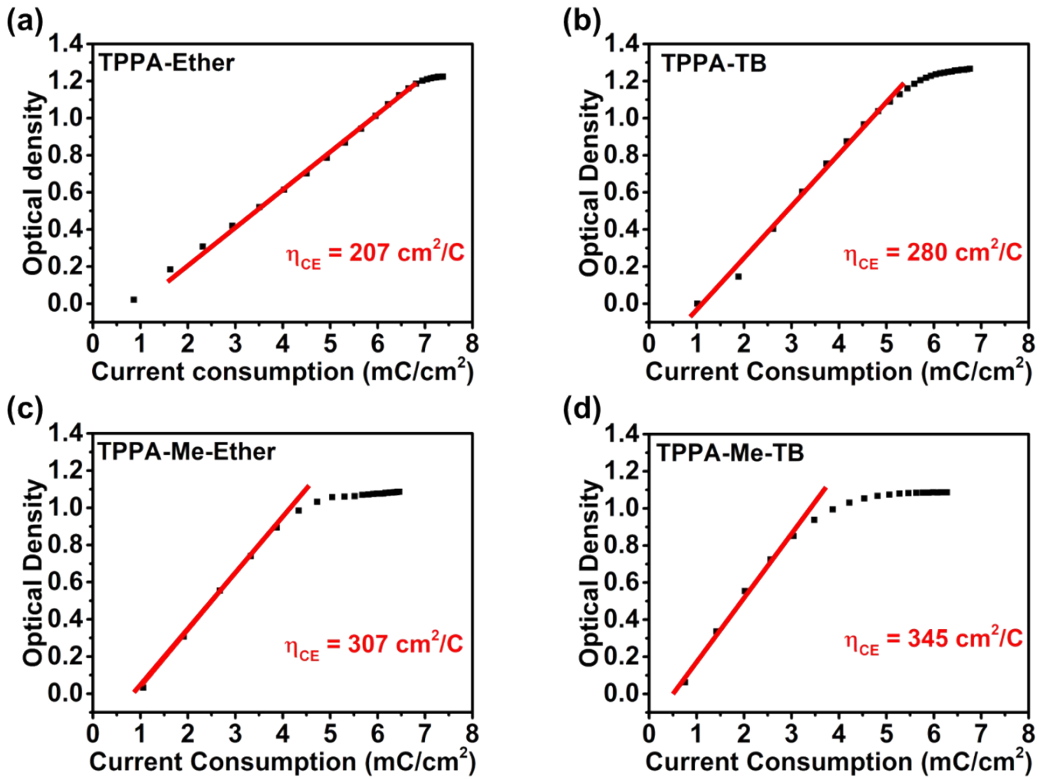

Fig. S30. The plots of optical density vs. current consumption of (a) **TPPA-Ether**, (b) **TPPA-TB**, (c) **TPPA-Me-Ether**, and (d) **TPPA-Me-TB** films on ITO glasses in 0.1M $TBABF_4$/MeCN to calculate the coloration efficiency.

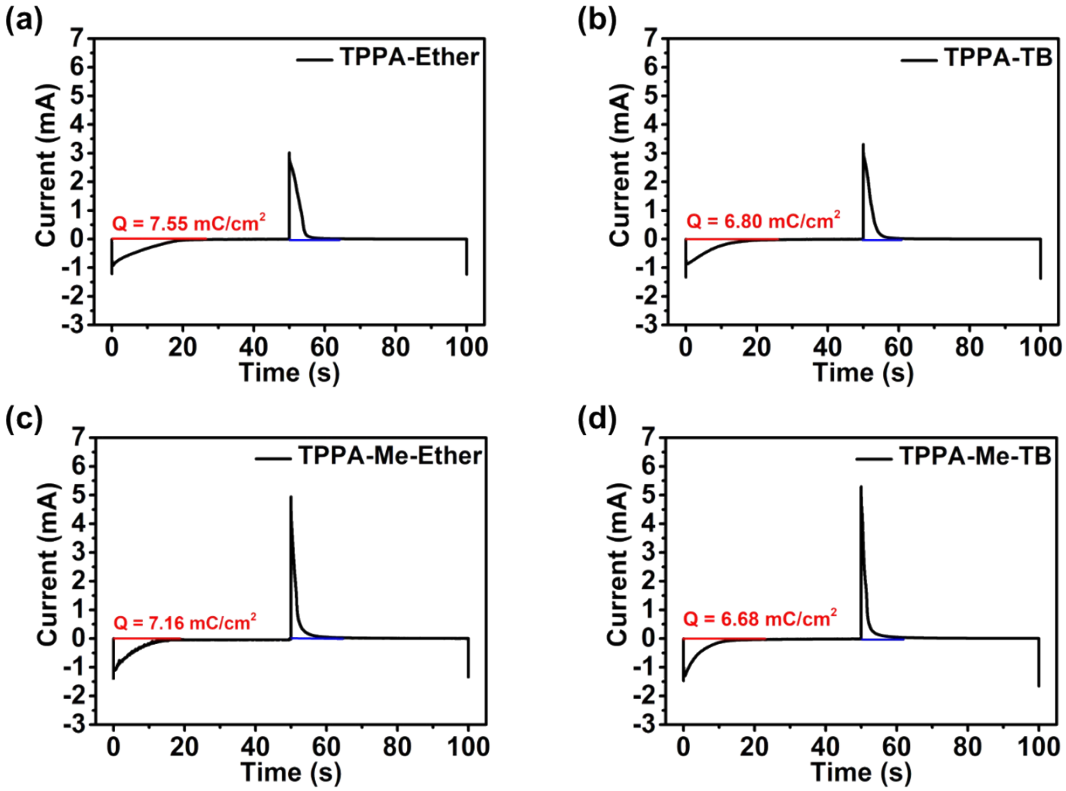

Fig. S31. Current consumption of (a) **TPPA-Ether**, (b) **TPPA-TB**, (c) **TPPA-Me-Ether**, and (d) **TPPA-Me-TB** films on ITO glasses with 0.8 V and -0.2 V as coloring and bleaching potentials in 0.1M $TBABF_4$/MeCN.

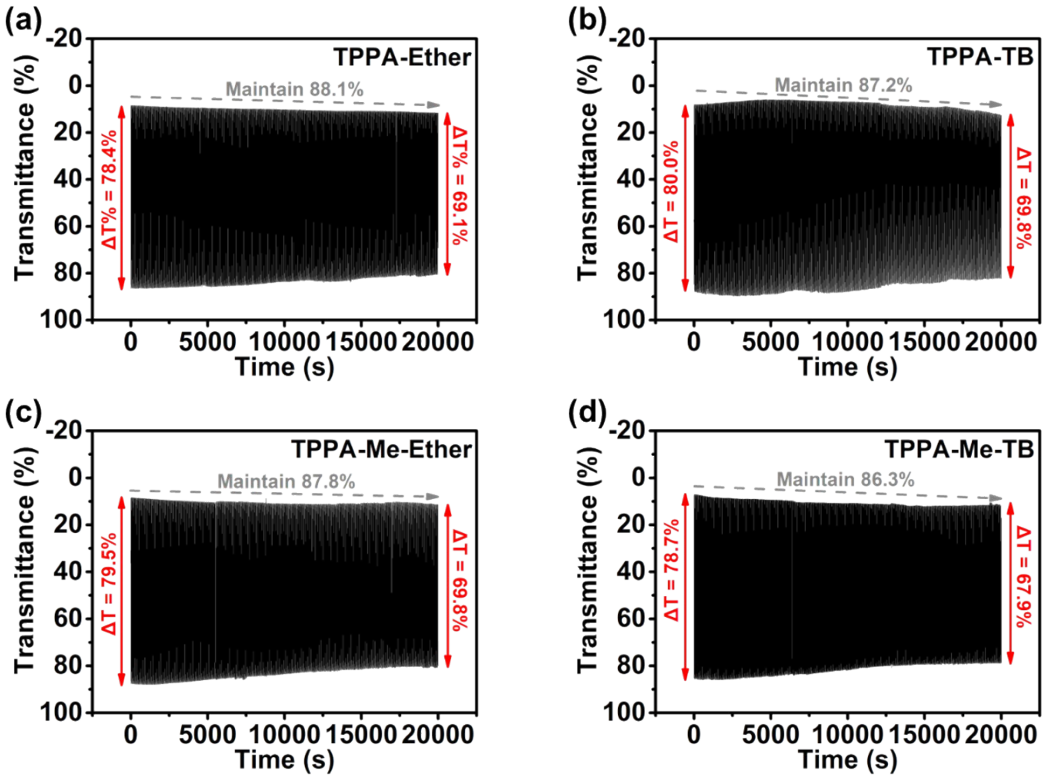

Fig. S32. Switching capability of prepared polymer films (thickness: 350 ± 30 nm) between 0.8 and −0.2 V at 433 nm with a cycle of 40 s for 500 cycles with 0.1 M $TBABF_4$ in 3 mL of MeCN.

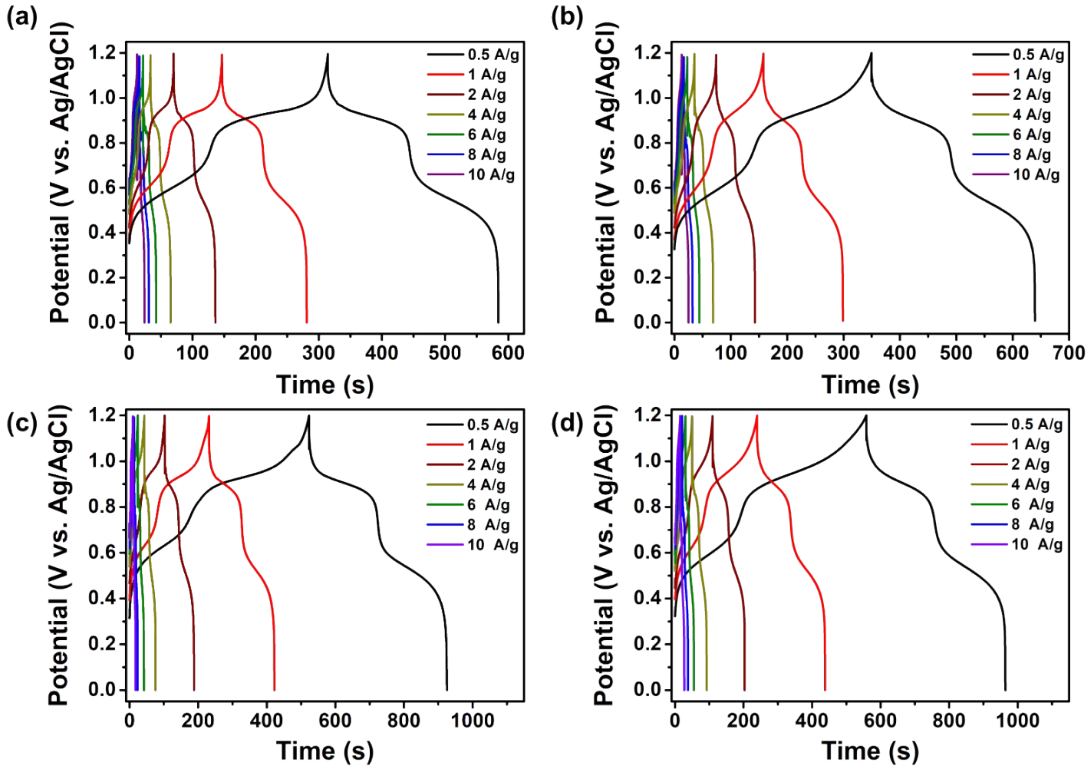

Fig. S33. Galvanostatic charge-discharge curves of (a) **TPPA-Ether**, (b) **TPPA-TB**, (c) **TPPA-Me-Ether**, and (d) **TPPA-Me-TB** films in a three-electrode configuration at different current densities in 0.1 M $TBABF_4$/MeCN.

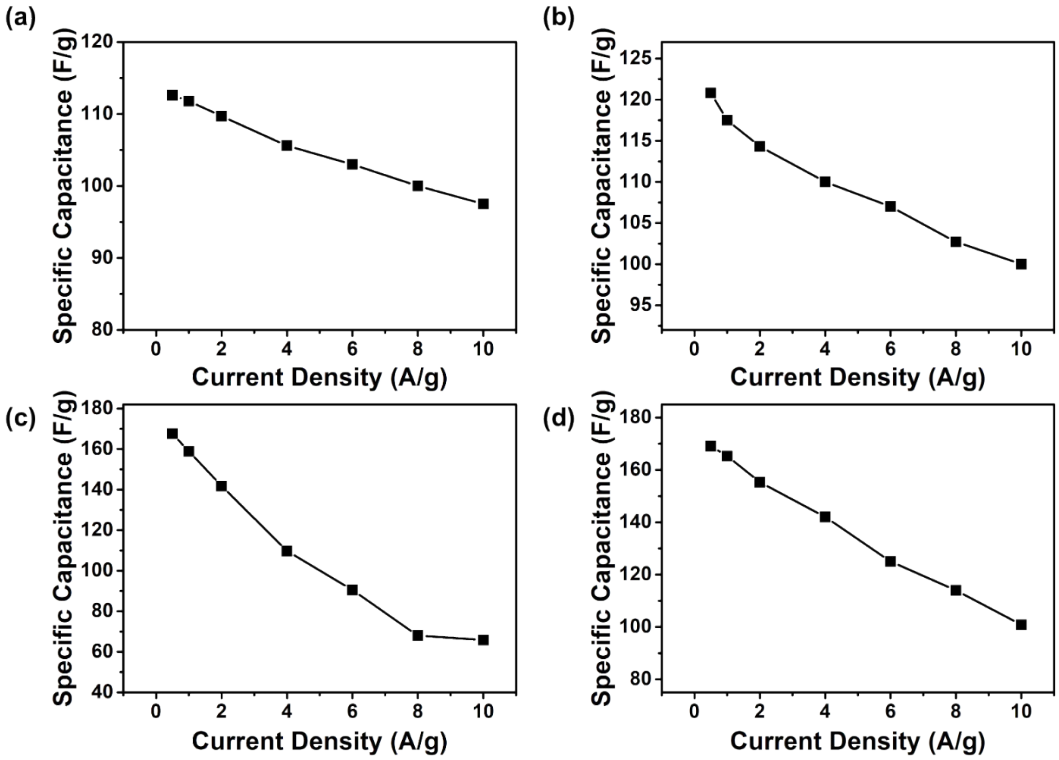

Fig. S34. Plots of the C_{sp} vs. different current densities for (a) **TPPA-Ether**, (b) **TPPA-TB**, (c) **TPPA-Me-Ether**, and (d) **TPPA-Me-TB**.

Table S1. Inherent viscosities and molecular weights of the TPPA-based polymers

Polymers	η_{inh} (dL/g) [a]	M_w (kDa) [b]	M_n (kDa) [b]	PDI [c]
TPPA-Ether	0.67	147.9	76.8	1.92
TPPA-Me-Ether	0.44	99.6	62.8	1.58
TPPA-TB	0.24	75.8	41.2	1.84
TPPA-Me-TB	0.35	114.1	58.0	1.97

[a] Measured at a concentration of 0.5 g/dL in DMAc at 30 ℃.

[b] Calibrated with polystyrene standards, using NMP as the eluent at a constant flow rate of 0.35 mL/min at 40 ℃.

[c] Polydispersity index = M_w/M_n.

Table S2. Solubility test of the TPPA-based polymers

Polymers	Solubility in Solvents [a]						
	NMP	**DMAc**	**DMF**	**DMSO**	***m*-Cresol**	**THF**	**$CHCl_3$**
TPPA-Ether	+ +	+ +	+ +	+ +	+ +	+ –	–
TPPA-TB	+ +	+ +	+ +	+ +	+ +	+ –	–
TPPA-Me-Ether	+ +	+ +	+ +	+ +	+ +	+ –	–
TPPA-Me-TB	+ +	+ +	+ +	+ +	+ +	+ –	–

[a] Measured at the concentration of 5 mg polymer in 1 mL specific solvent. + +: dissolved at room temperature; +: dissolved after heating; + –: partially dissolved after heating; –: not dissolved.

Table S3. Switching response time of the TPPA-based polymer films

Polymer [a]	t_c (s) [a]	δt_c (s) [b]	δt_c (%) [c]	t_b (s) [d]	δt_b (s) [e]	δt_b (%) [f]
TPPA-Ether	8.1	-	-	4.3	-	-
TPPA-TB	7.8	0.3	3.7	3.6	0.7	16.3
TPPA-Me-Ether	4.6	3.5	43.2	3.8	0.5	11.6
TPPA-Me-TB	4.4	3.7	45.7	2.2	2.1	48.8

[a] Coloring time from a neutral state to 90% of optical change (thickness: 350 ± 30 nm).

[b] The difference in coloring time compared with **TPPA-Ether**.

[c] The percentage of decreasing coloring time compared with **TPPA-Ether**.

[d] Bleaching time from coloring state to 90% of optical change.

[e] The difference in bleaching time compared with **TPPA-Ether**.

[f] The percentage of decreasing bleaching time compared with **TPPA-Ether**.

Table S4 C_{sp} value of the **TPPA-**based polymer films at the different current density

Polymer	Specific Capacitance (F/g) [a]						
	0.5 (A/g)	**1 (A/g)**	**2 (A/g)**	**4 (A/g)**	**6 (A/g)**	**8 (A/g)**	**10 (A/g)**
TPPA-Ether	112.6	111.8	109.7	105.6	103.0	100.0	97.5
TPPA-TB	120.8	117.5	114.3	110.0	107.0	102.7	100.0
TPPA-Me-Ether	167.6	158.9	141.8	109.7	90.5	68.0	65.8
TPPA-Me-TB	169.1	165.3	155.3	142.0	125.0	114.0	100.8

[a] Specific capacitance (C_{sp}) is calculated by $C_{sp} = \frac{I \times \Delta t_{discharge}}{m \times \Delta V}$.